Electronic Supplementary Information

Post-synthetic modification of zeolitic imidazolate framework-90 via Schiff base reaction for ultrahigh iodine capture

Zilong Zhang,[†a] Yanchun Chen,[†a] Yiheng Sun,[a] Zilu Chen,*[a] Zhan-Yun Zhang,*[a] Fupei Liang,[a,b] Dongcheng Liu,[a] and Huan-Cheng Hu*[a]

[a]*School of Chemistry and Pharmaceutical Sciences, State Key Laboratory for Chemistry and Molecular Engineering of Medicinal Resources, Guangxi Normal University, Guilin, 541004, People's Republic of China.*

[b]*Guangxi Key Laboratory of Electrochemical and Magnetochemical Functional Materials, College of Chemistry and Bioengineering, Guilin University of Technology, Guilin, 541004, People's Republic of China.*

*Corresponding author

E-mail: zlchen@mailbox.gxnu.edu.cn (Z. Chen); zhang_zhanyun@126.com (Z.-Y. Zhang); siniantongnian@126.com (H.-C. Hu)

† These authors contributed equally to this work.

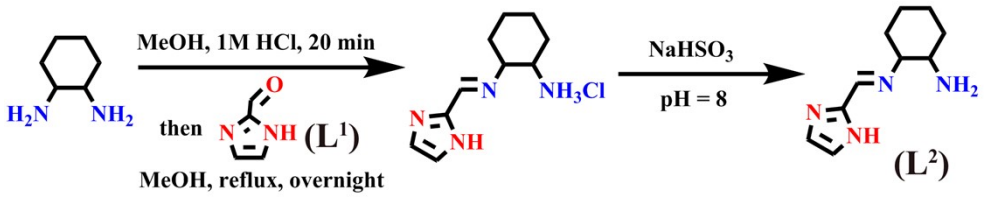

Scheme S1 Synthesis route of mono-Schiff base.

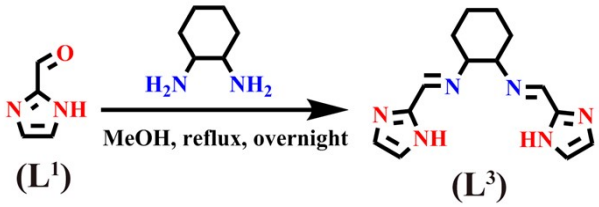

Scheme S2 Synthesis route of bis-Schiff base.

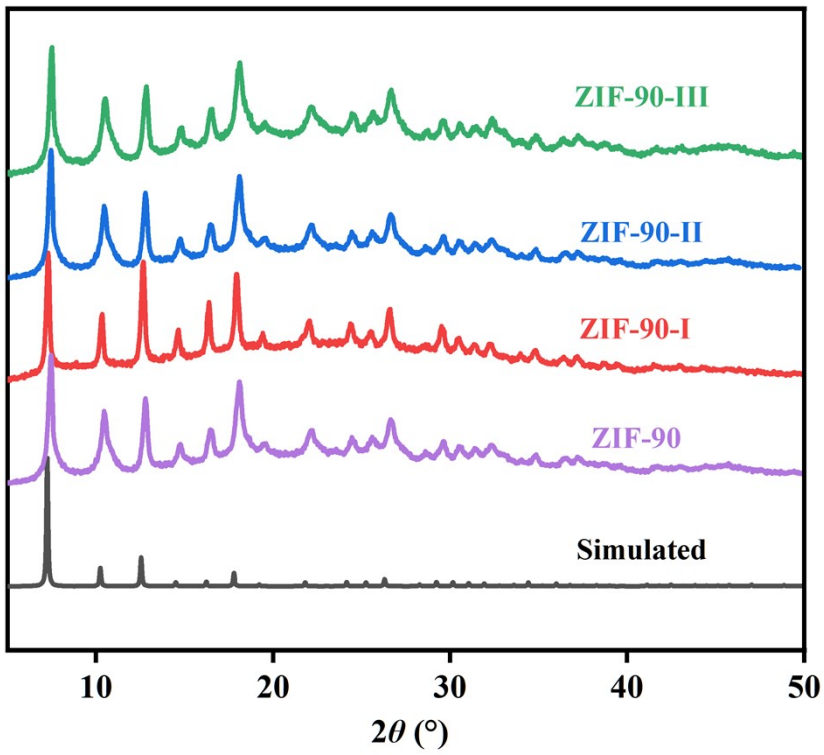

Fig. S1 PXRD patterns of simulated and experimental **ZIF-90** and **ZIF-90-I**–**ZIF-90-III**.

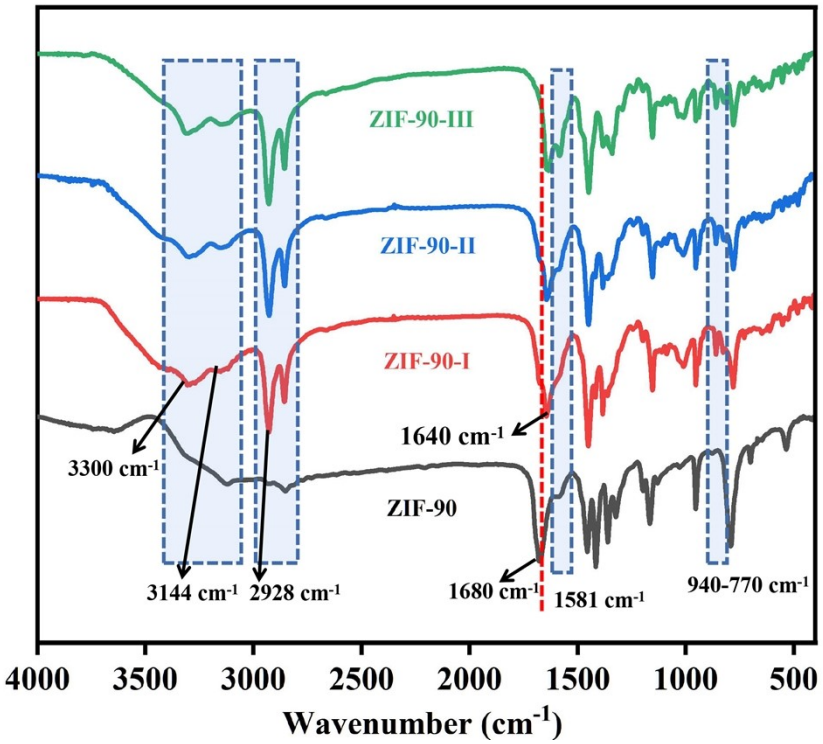

Fig. S2 FTIR spectra of **ZIF-90** and **ZIF-90-I**–**ZIF-90-III**.

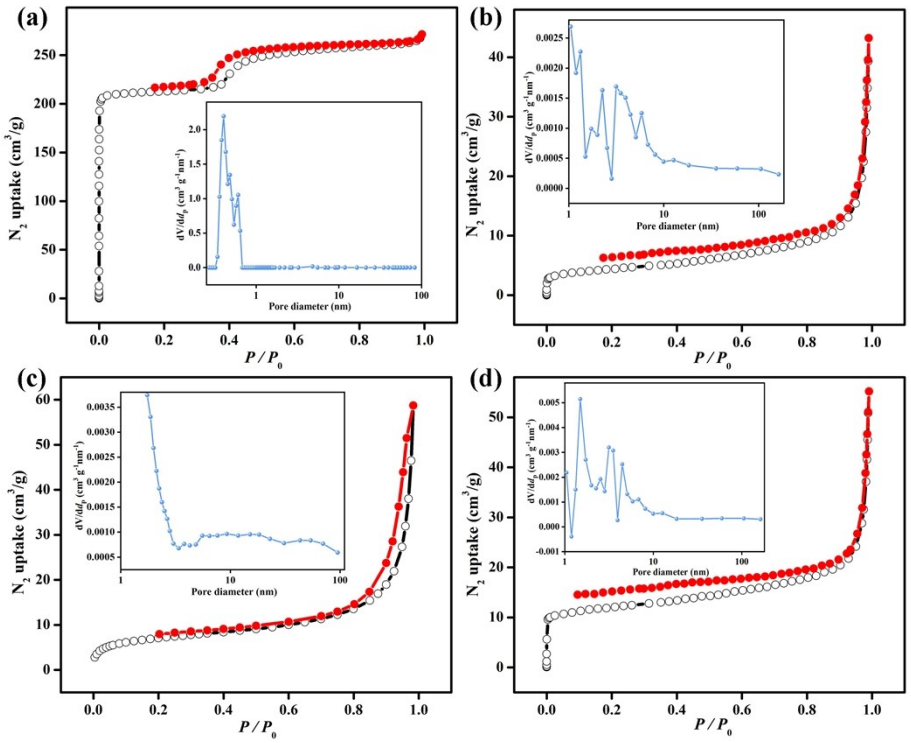

Fig. S3 N_2 adsorption-desorption isotherms for activated samples of (a) **ZIF-90**, (b) **ZIF-90-I** (c) **ZIF-90-II** and (d) **ZIF-90-III** measured at 77 K. Enlargement: Pore size distributions of **ZIF-90** and **ZIF-90-I**–**ZIF-90-III**.

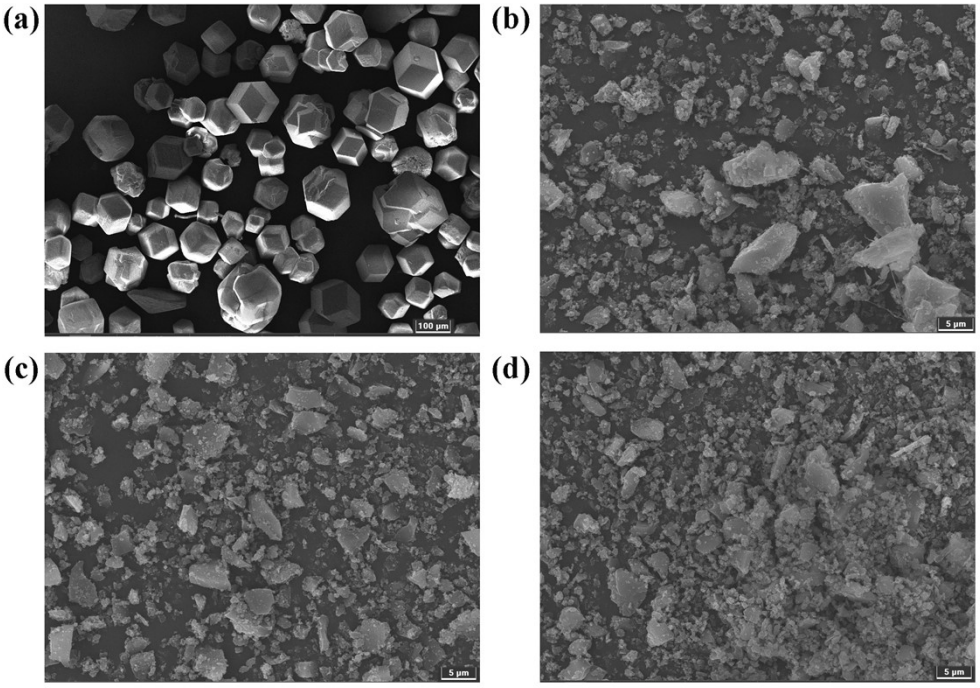

Fig. S4 SEM images of (a) **ZIF-90**, (b) **ZIF-90-I**, (c) **ZIF-90-II** and (d) **ZIF-90-III**.

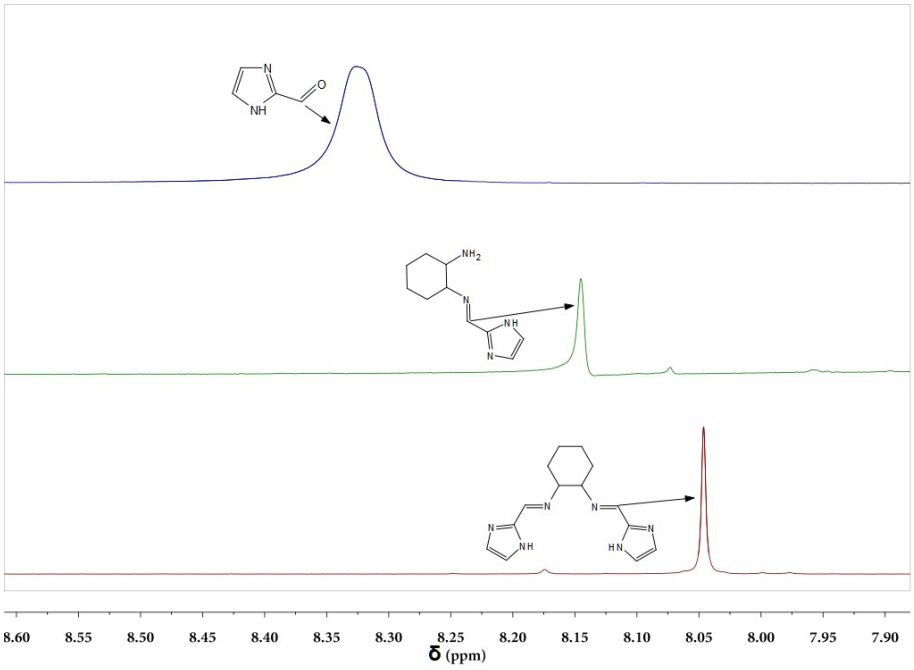

Fig. S5 ^{1}H NMR of L^{1}, L^{2} and L^{3}.

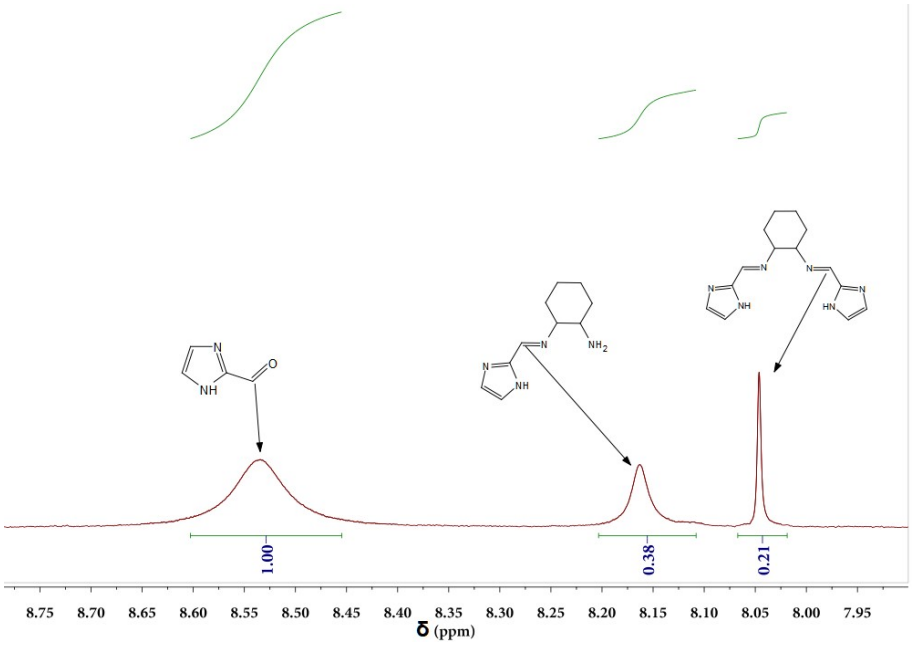

Fig. S6 ^{1}H NMR of digested **ZIF-90-I**.

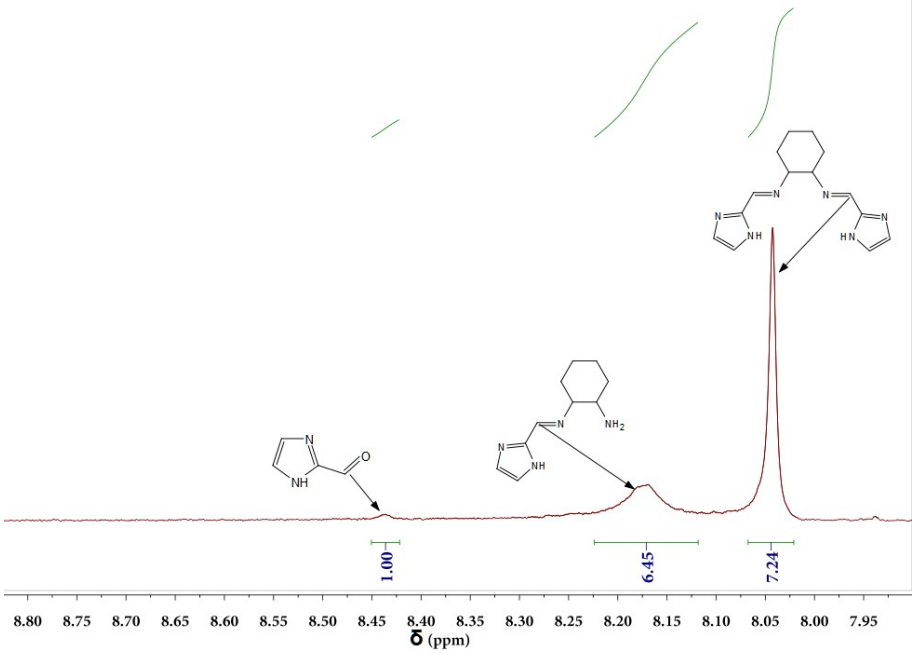

Fig. S7 ^{1}H NMR of digested **ZIF-90-II**.

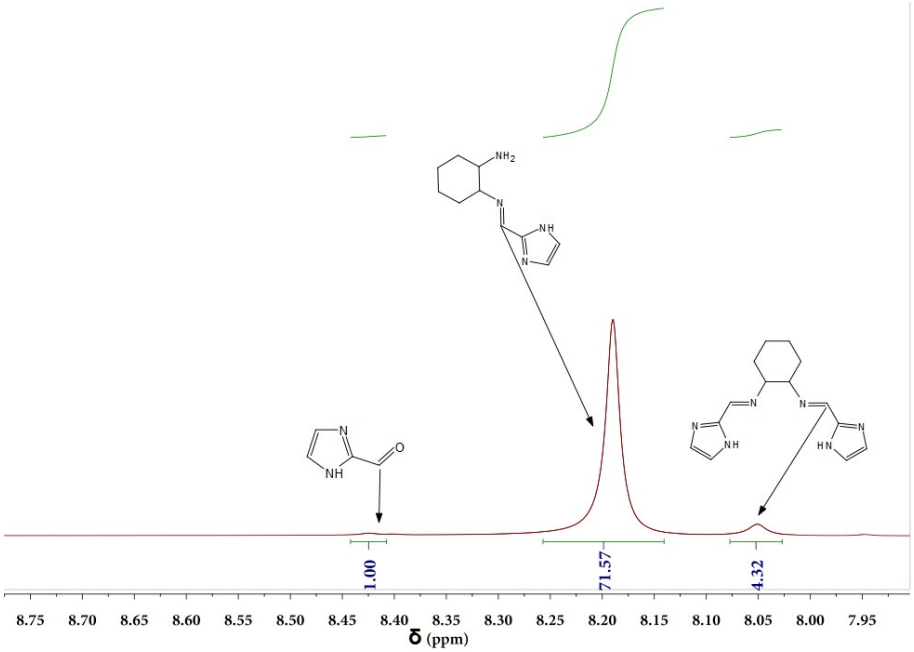

Fig. S8 ^{1}H NMR of digested **ZIF-90-III**.

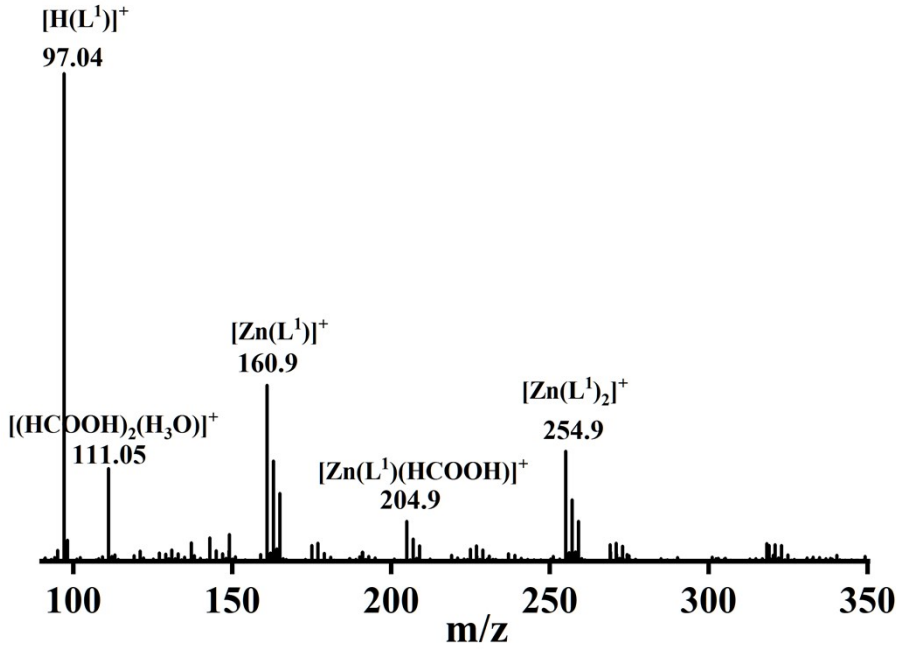

Fig. S9 HRESI-MS of digested **ZIF-90**.

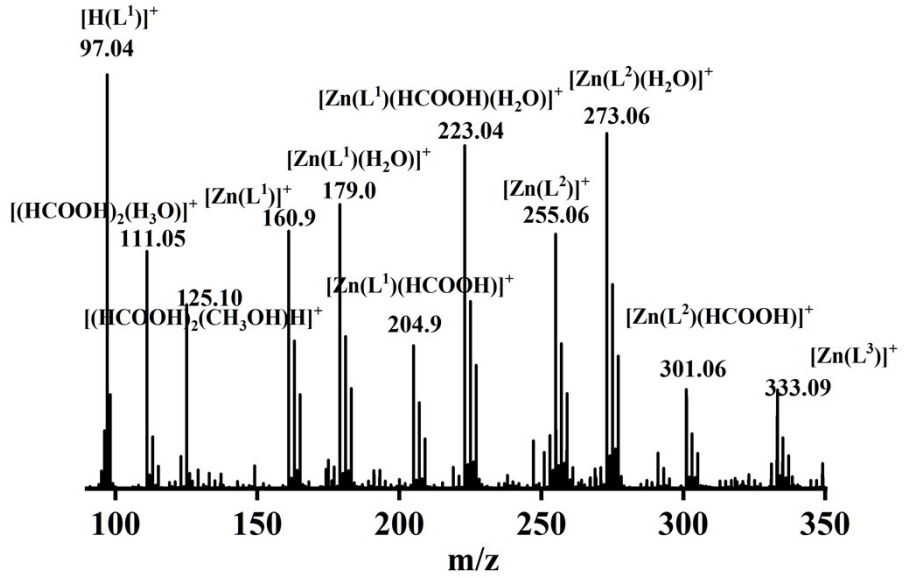

Fig. S10 HRESI-MS of digested **ZIF-90-I**.

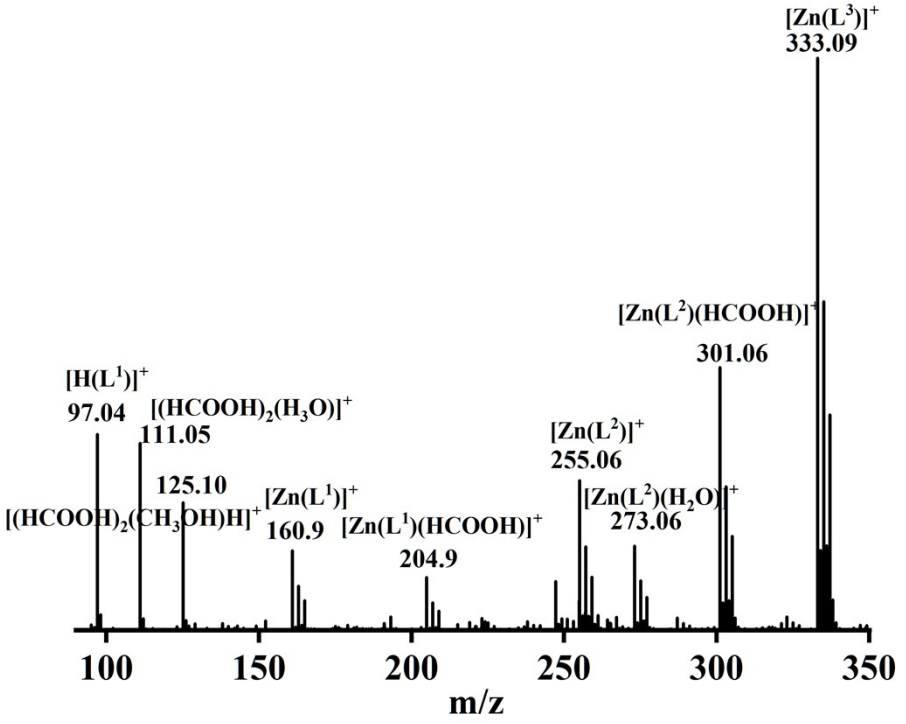

Fig. S11 HRESI-MS of digested **ZIF-90-II**.

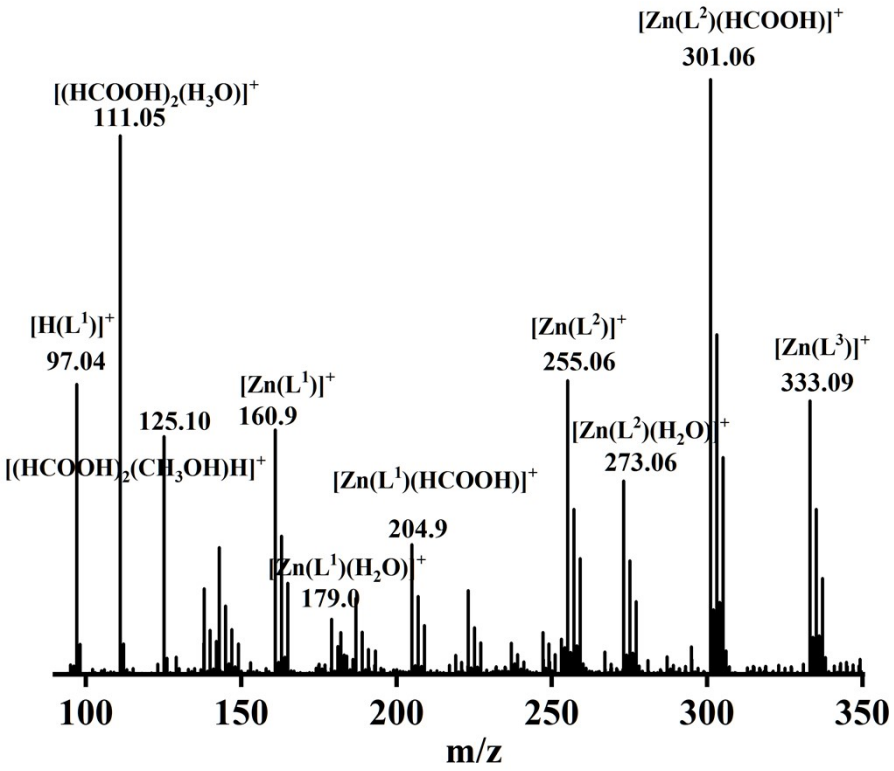

Fig. S12 HRESI-MS of digested **ZIF-90-III**.

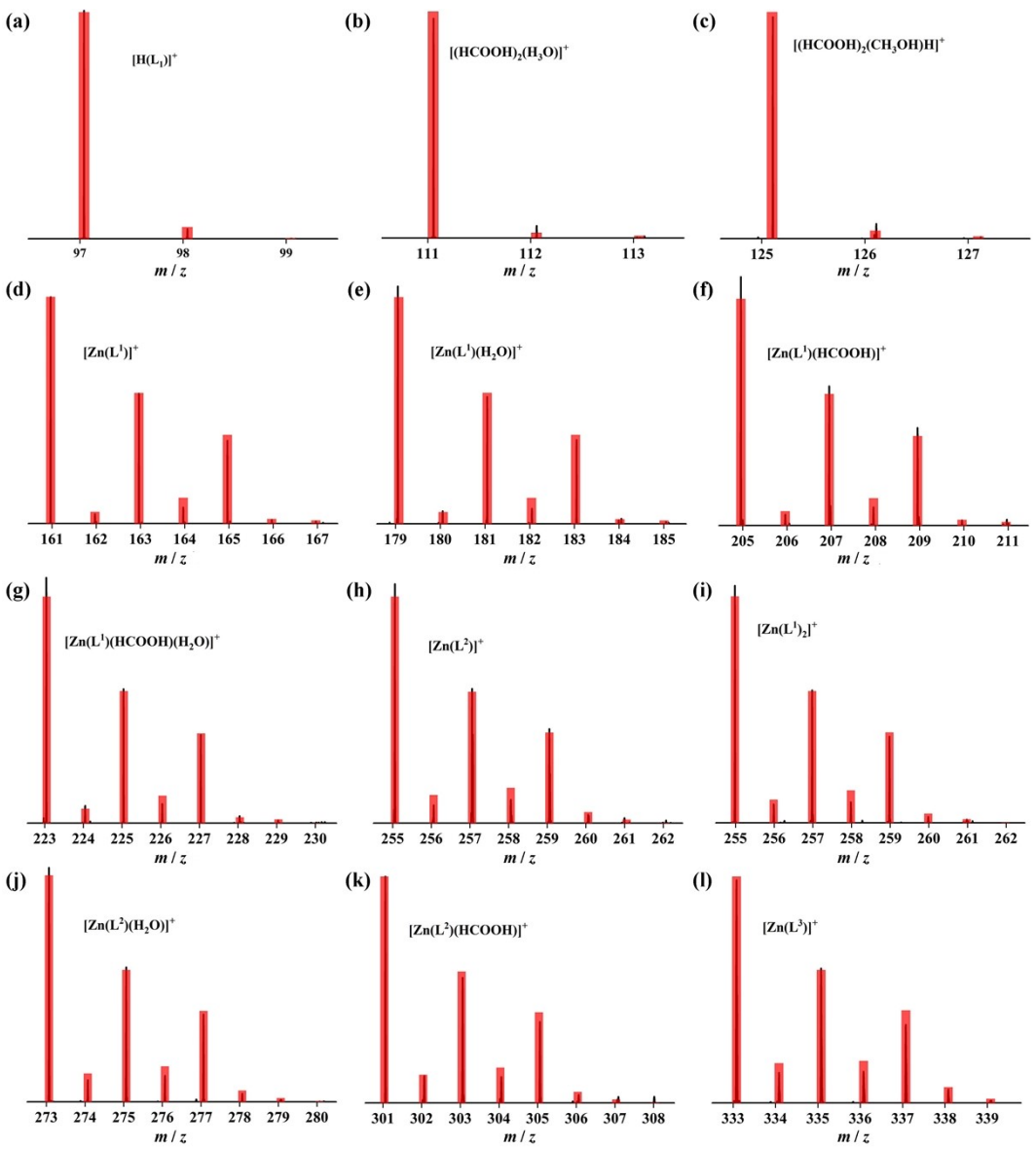

Fig. S13 The superposed simulated and observed HRESI-MS spectra of major species for digested **ZIF-90-I**–**ZIF-90-III**.

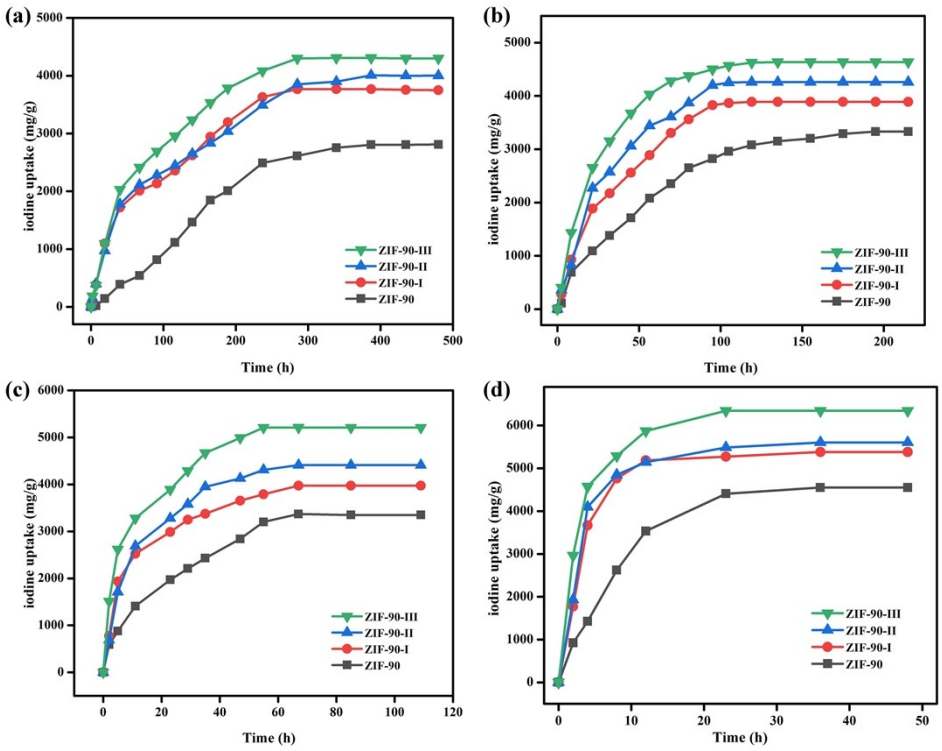

Fig. S14 Iodine adsorption isotherms of **ZIF-90** and **ZIF-90-I**–**ZIF-90-III** at (a) 40, (b) 50, (c) 60 and (d) 90 ºC under ambient pressure.

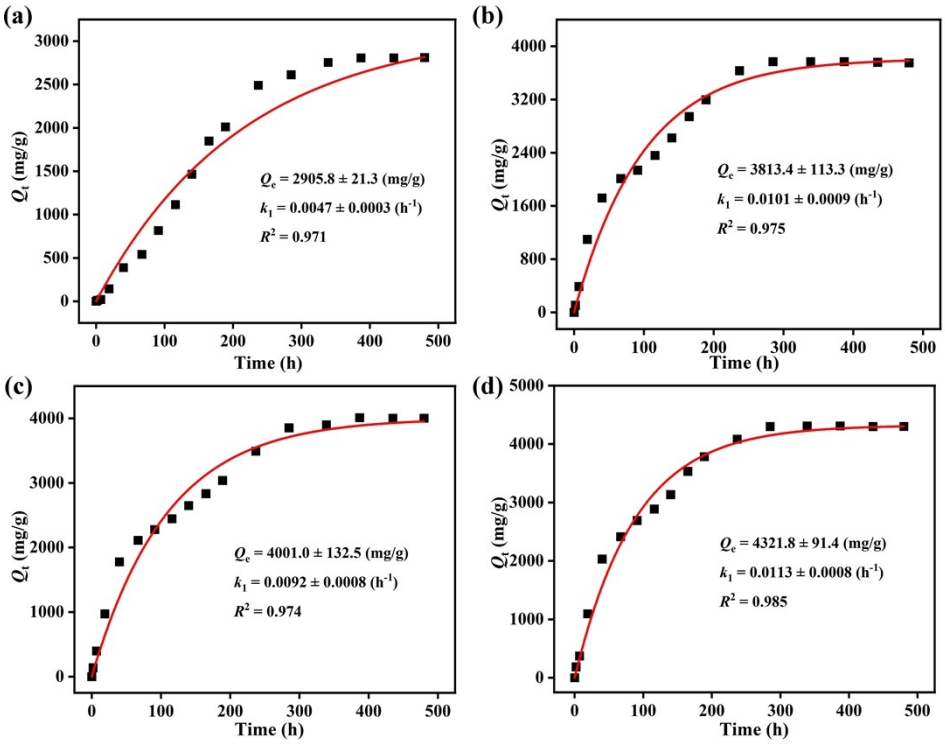

Fig. S15 The pseudo-first kinetic models for iodine vapour adsorption kinetics of (a) **ZIF-90**, (b) **ZIF-90-I**, (c) **ZIF-90-II** and (d) **ZIF-90-III** at 40 ºC under ambient pressure.

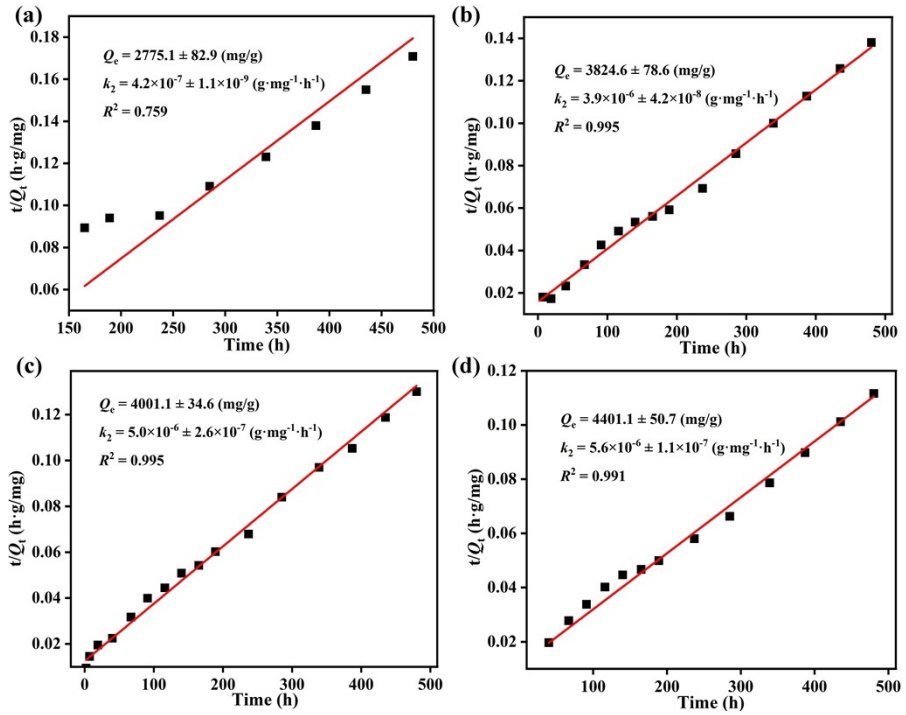

Fig. S16 The pseudo-second kinetic models for iodine vapour adsorption kinetics of (a) **ZIF-90**, (b) **ZIF-90-I**, (c) **ZIF-90-II** and (d) **ZIF-90-III** at 40 ºC under ambient pressure.

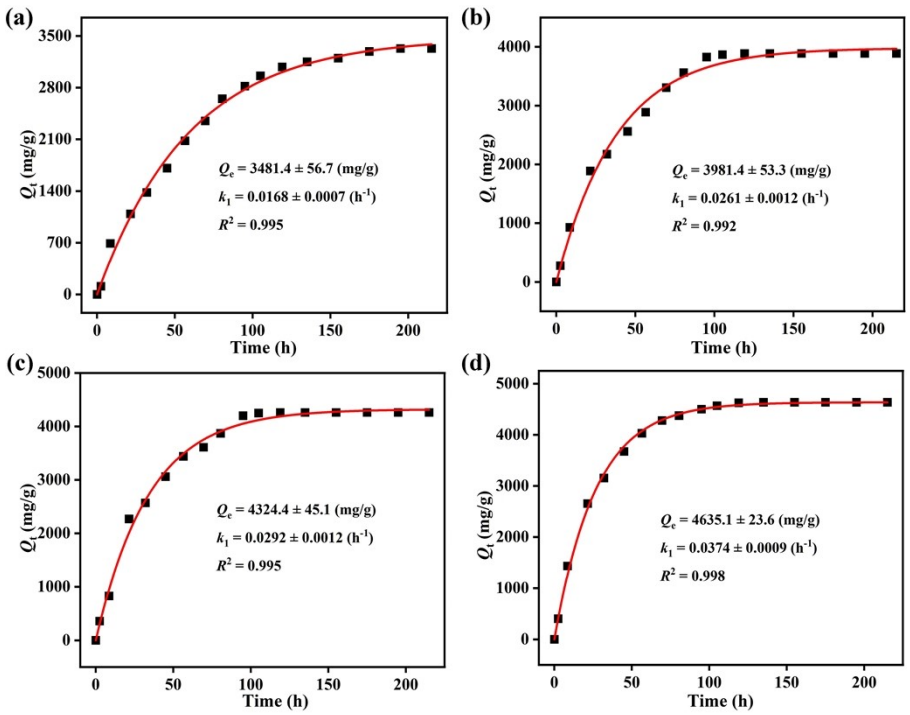

Fig. S17 The pseudo-first kinetic models for iodine vapour adsorption kinetics of (a) **ZIF-90**, (b) **ZIF-90-I**, (c) **ZIF-90-II** and (d) **ZIF-90-III** at 50 ºC under ambient pressure.

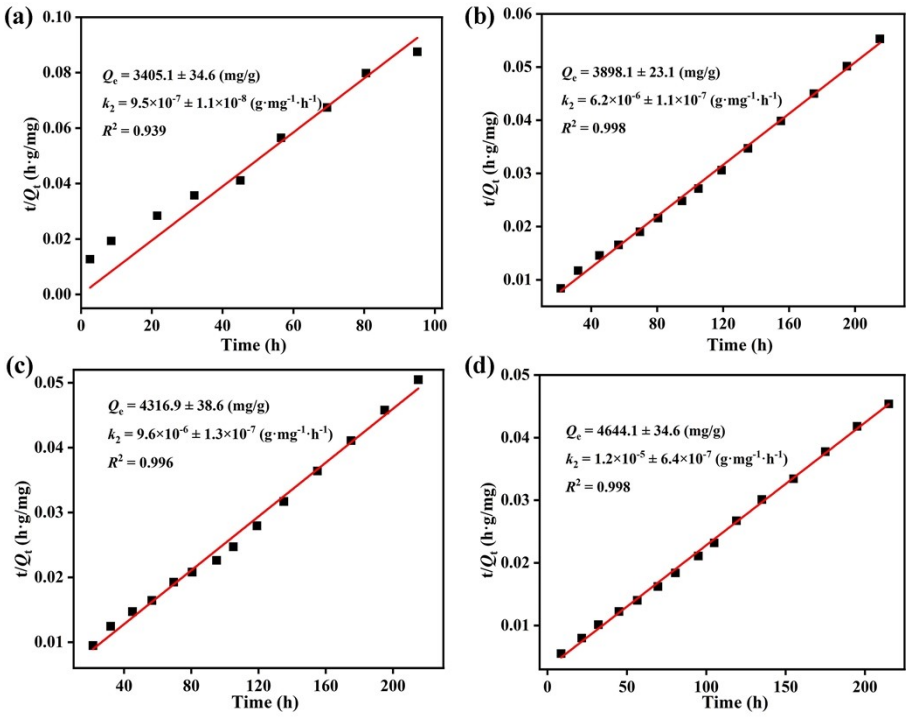

Fig. S18 The pseudo-second kinetic models for iodine vapour adsorption kinetics of (a) **ZIF-90**, (b) **ZIF-90-I**, (c) **ZIF-90-II** and (d) **ZIF-90-III** at 50 ºC under ambient pressure.

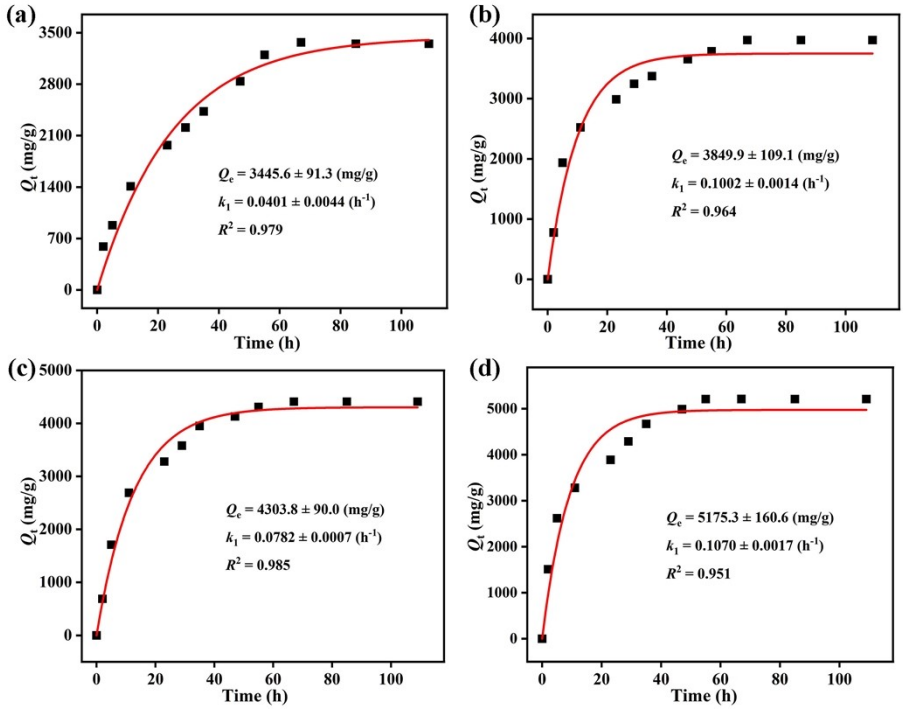

Fig. S19 The pseudo-first kinetic models for iodine vapour adsorption kinetics of (a) **ZIF-90**, (b) **ZIF-90-I**, (c) **ZIF-90-II** and (d) **ZIF-90-III** at 60 ºC under ambient pressure.

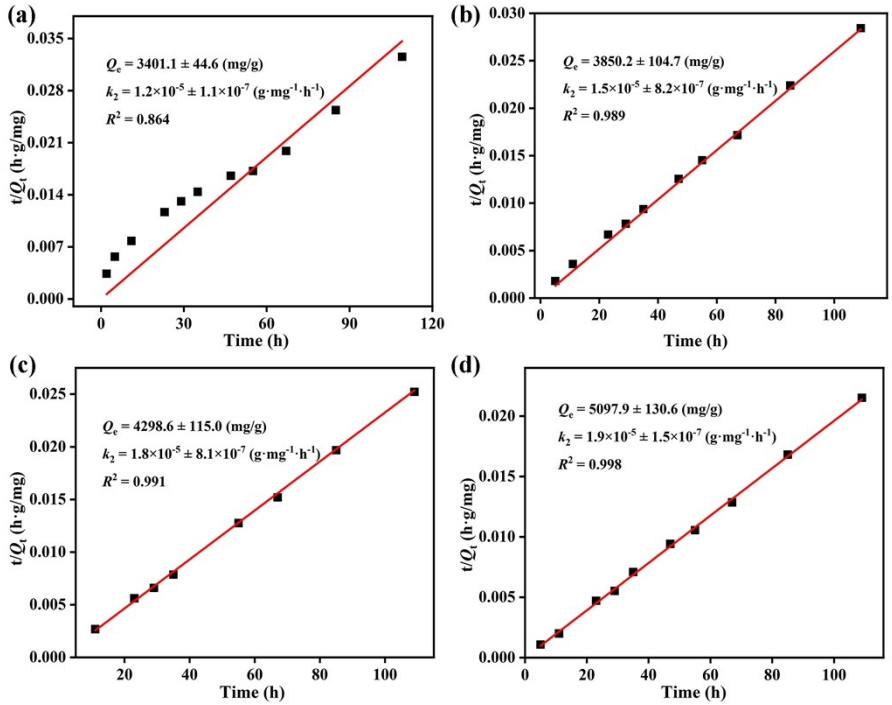

Fig. S20 The pseudo-second kinetic models for iodine vapour adsorption kinetics of (a) **ZIF-90**, (b) **ZIF-90-I**, (c) **ZIF-90-II** and (d) **ZIF-90-III** at 60 ºC under ambient pressure.

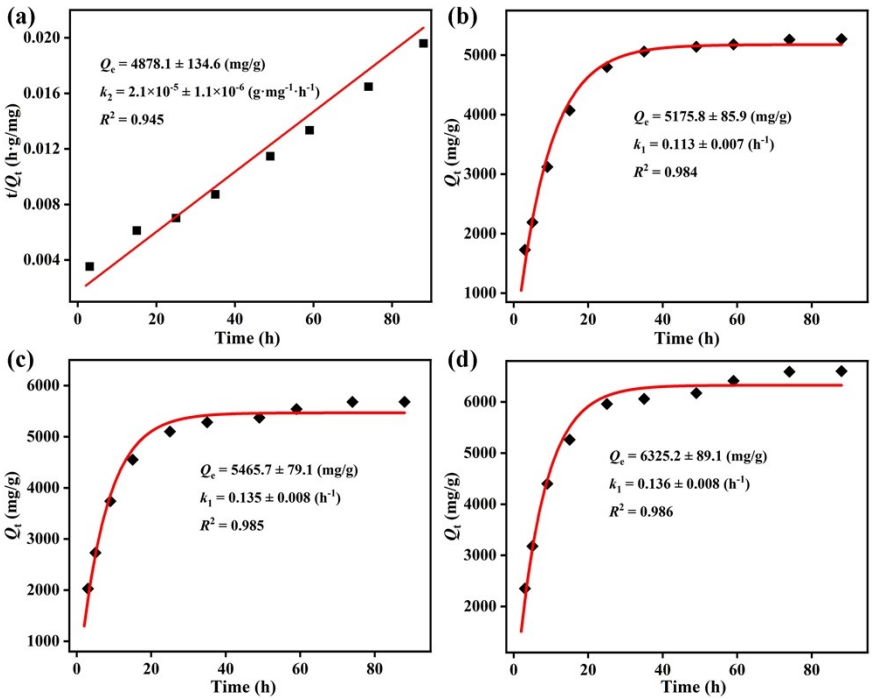

Fig. S21 The pseudo-second kinetic models for iodine vapor adsorption kinetics of (a) **ZIF-90**, the pseudo-first kinetic models for iodine vapor adsorption kinetics of (b) **ZIF-90-I**, (c) **ZIF-90-II** and (d) **ZIF-90-III** at 75 ºC under ambient pressure.

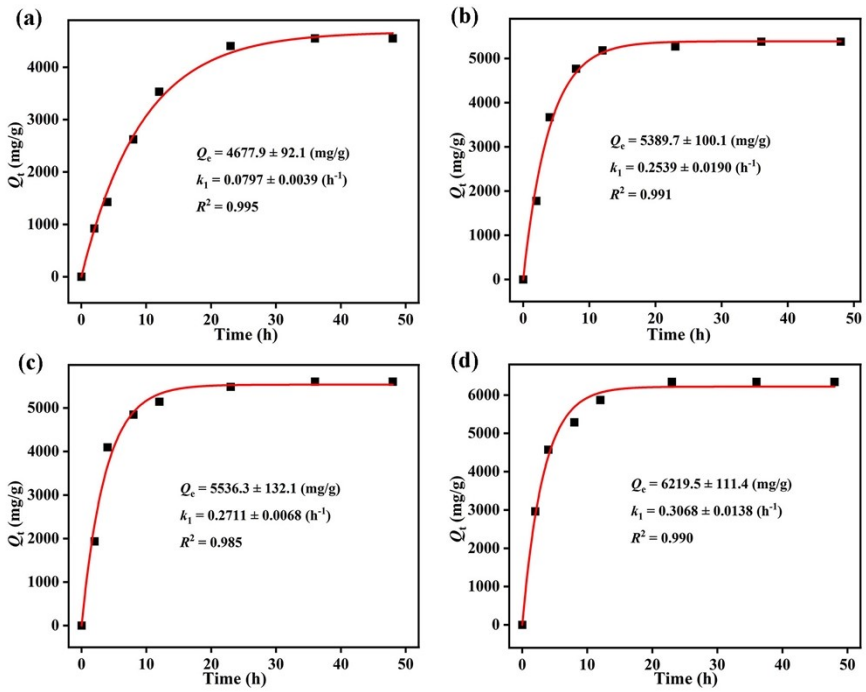

Fig. S22 The pseudo-first kinetic models for iodine vapour adsorption kinetics of (a) **ZIF-90**, (b) **ZIF-90-I**, (c) **ZIF-90-II** and (d) **ZIF-90-III** at 90 ºC under ambient pressure.

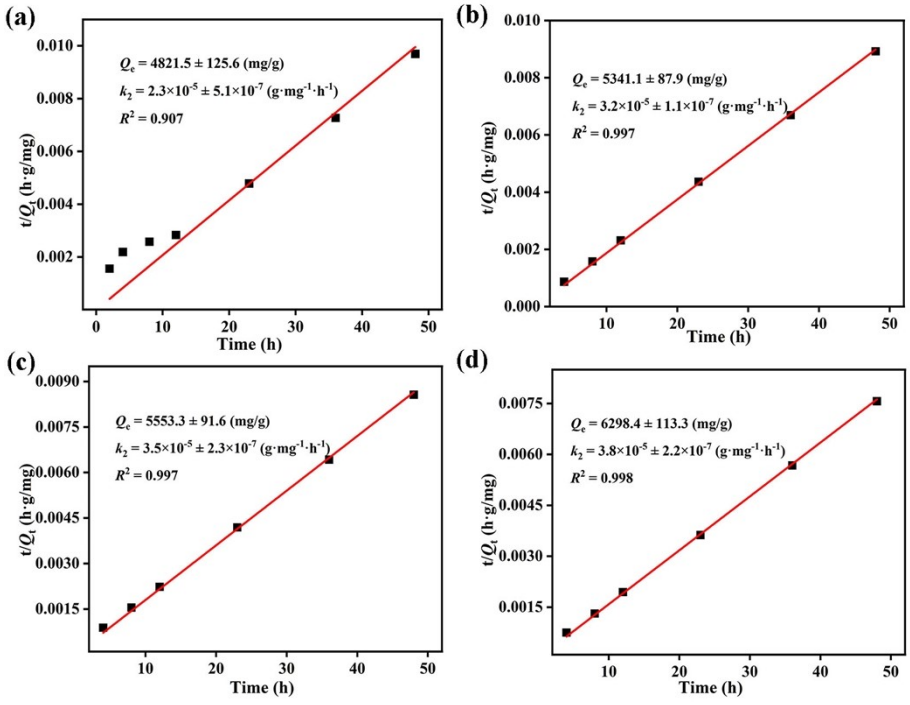

Fig. S23 The pseudo-second kinetic models for iodine vapour adsorption kinetics of (a) **ZIF-90**, (b) **ZIF-90-I**, (c) **ZIF-90-II** and (d) **ZIF-90-III** at 90 ºC under ambient pressure.

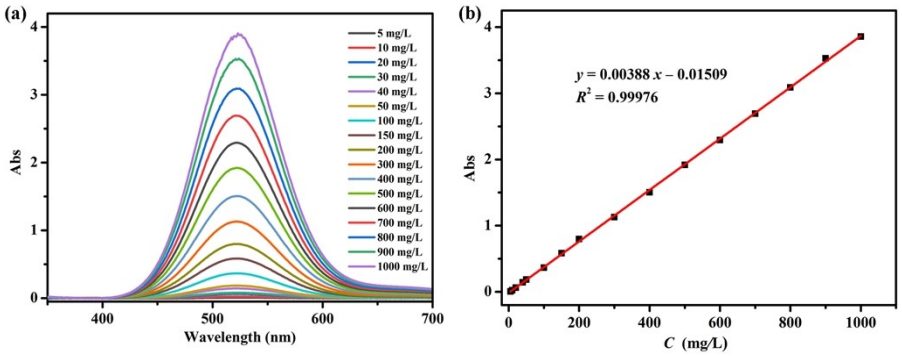

Fig. S24 The standard curve of iodine/cyclohexane solution.

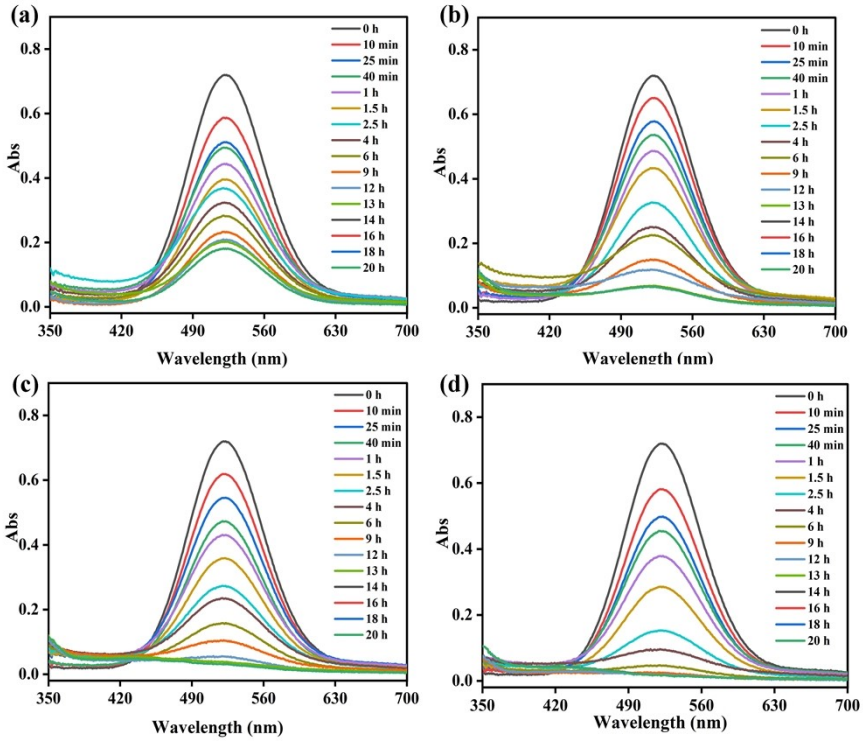

Fig. S25 Temporal evolution of UV-vis absorption spectra for iodine adsorption by (a) **ZIF-90**, (b) **ZIF-90-I**, (c) **ZIF-90-II** and (d) **ZIF-90-III** in 5 mL of 200 mg/L iodine/cyclohexane solution.

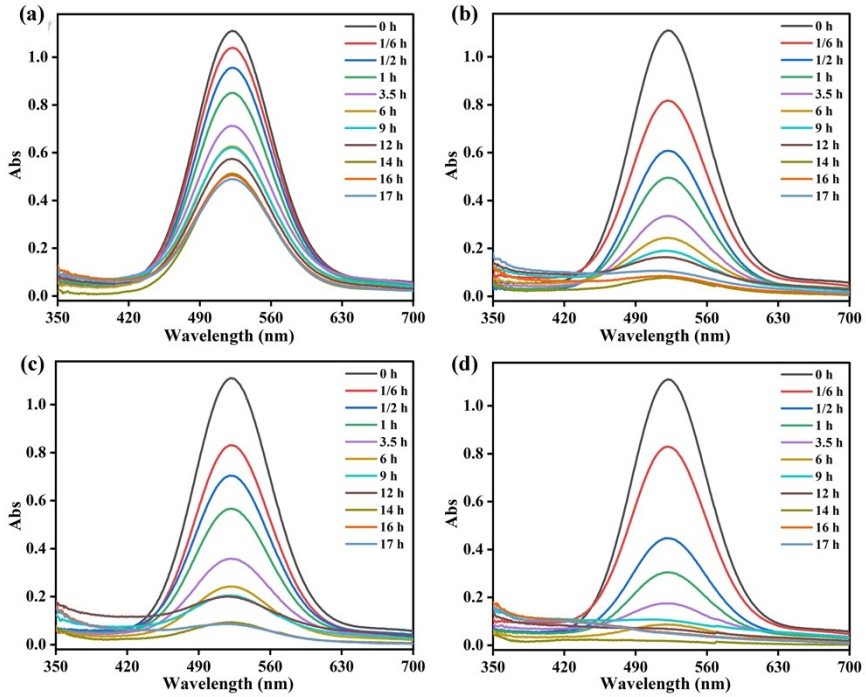

Fig. S26 Temporal evolution of UV-vis absorption spectra for iodine adsorption by (a) **ZIF-90**, (b) **ZIF-90-I**, (c) **ZIF-90-II** and (d) **ZIF-90-III** in 5 mL of 300 mg/L iodine/cyclohexane solution.

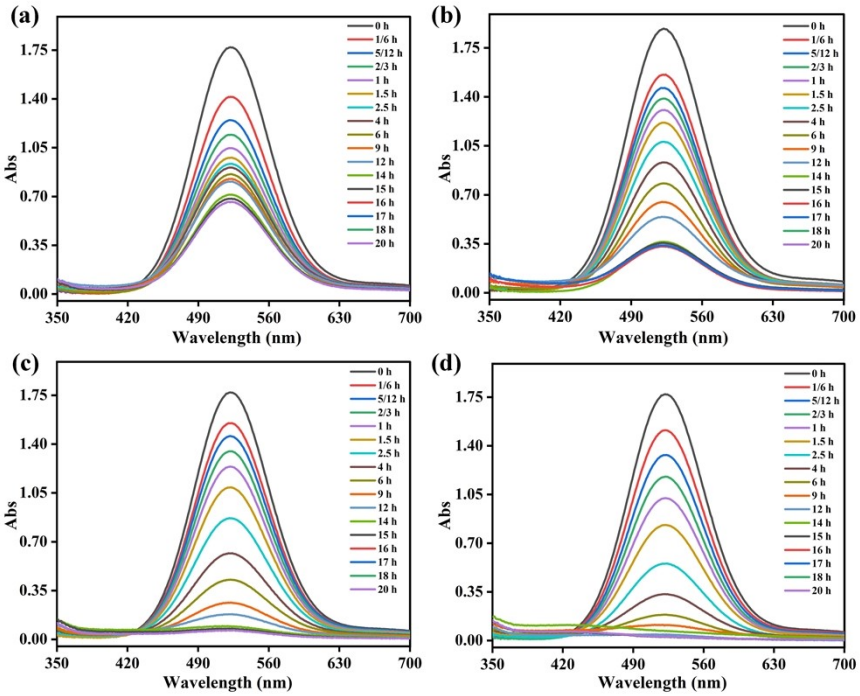

Fig. S27 Temporal evolution of UV-vis absorption spectra for iodine adsorption by (a) **ZIF-90**, (b) **ZIF-90-I**, (c) **ZIF-90-II** and (d) **ZIF-90-III** in 5 mL of 500 mg/L iodine/cyclohexane solution.

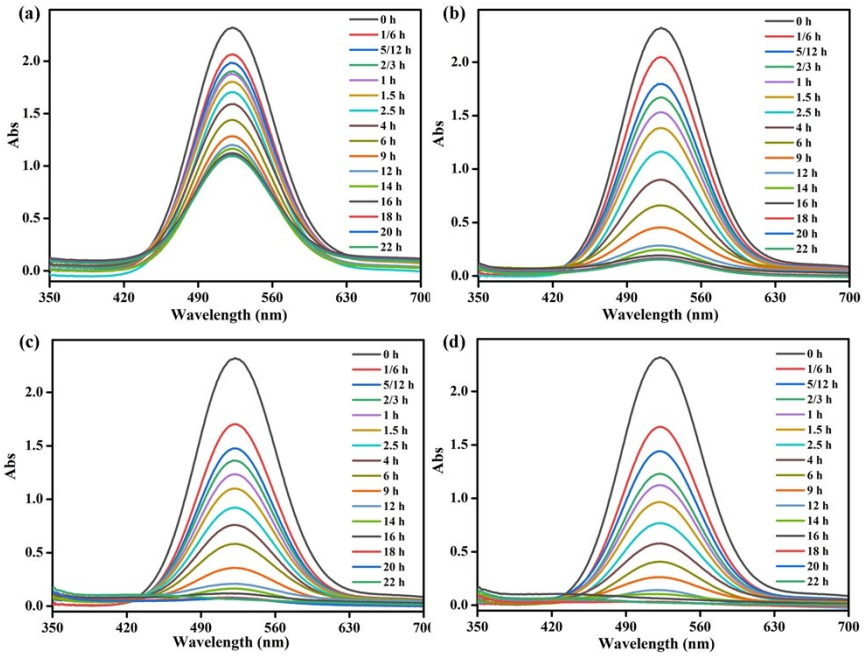

Fig. S28 Temporal evolution of UV-vis absorption spectra for iodine adsorption by (a) **ZIF-90**, (b) **ZIF-90-I**, (c) **ZIF-90-II** and (d) **ZIF-90-III** in 5 mL of 600 mg/L iodine/cyclohexane solution.

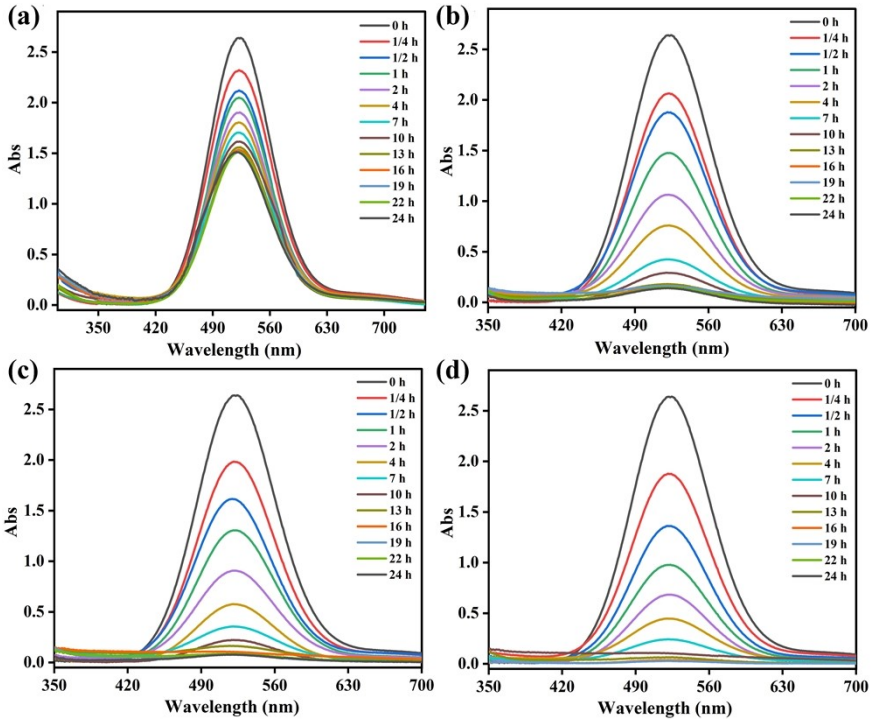

Fig. S29 Temporal evolution of UV-vis absorption spectra for iodine adsorption by (a) **ZIF-90**, (b) **ZIF-90-I**, (c) **ZIF-90-II** and (d) **ZIF-90-III** in 5 mL of 800 mg/L iodine/cyclohexane solution.

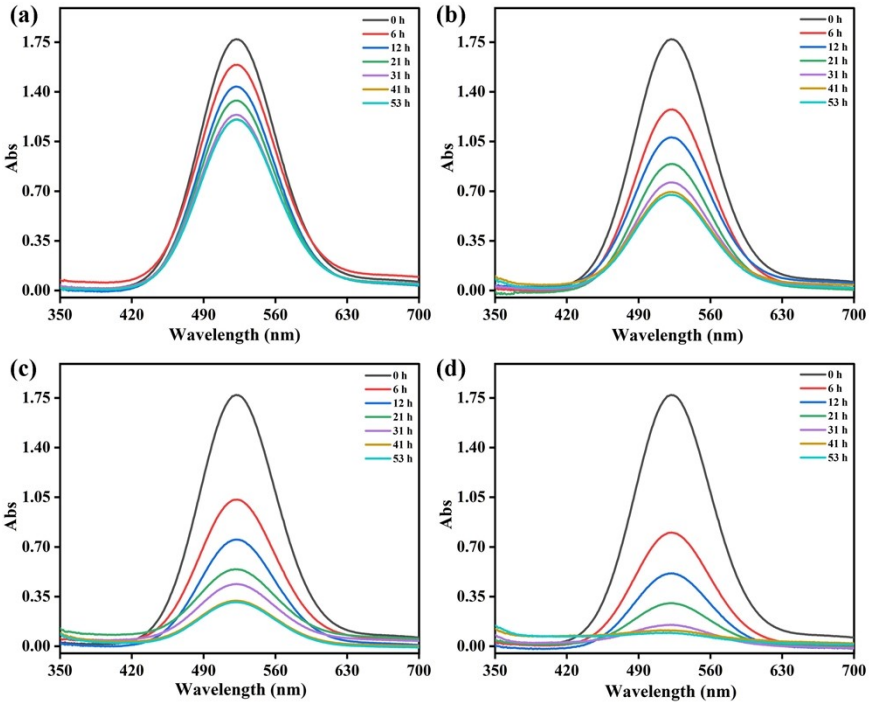

Fig. S30 Temporal evolution of UV-vis absorption spectra for iodine adsorption by (a) **ZIF-90**, (b) **ZIF-90-I**, (c) **ZIF-90-II** and (d) **ZIF-90-III** in 15 mL of 500 mg/L iodine/cyclohexane solution.

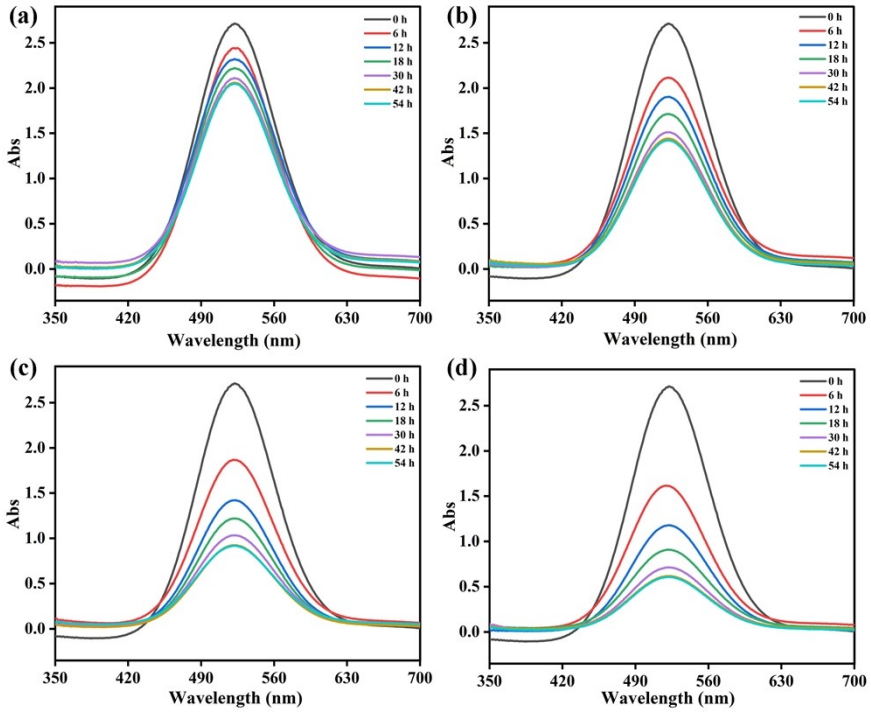

Fig. S31 Temporal evolution of UV-vis absorption spectra for iodine adsorption by (a) **ZIF-90**, (b) **ZIF-90-I**, (c) **ZIF-90-II** and (d) **ZIF-90-III** in 15 mL of 700 mg/L iodine/cyclohexane solution.

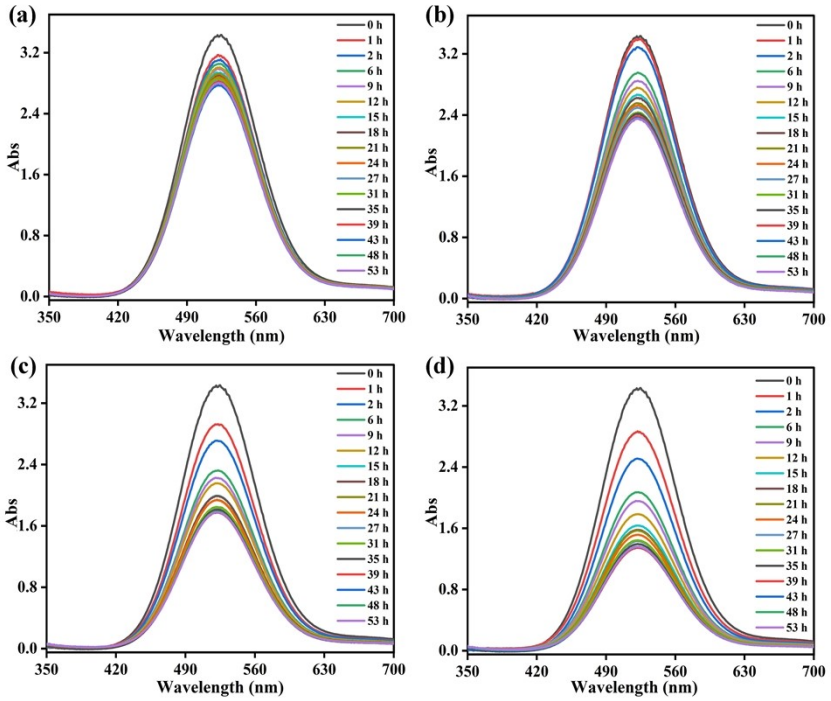

Fig. S32 Temporal evolution of UV-vis absorption spectra for iodine adsorption by (a) **ZIF-90**, (b) **ZIF-90-I**, (c) **ZIF-90-II** and (d) **ZIF-90-III** in 15 mL of 1000 mg/L iodine/cyclohexane solution.

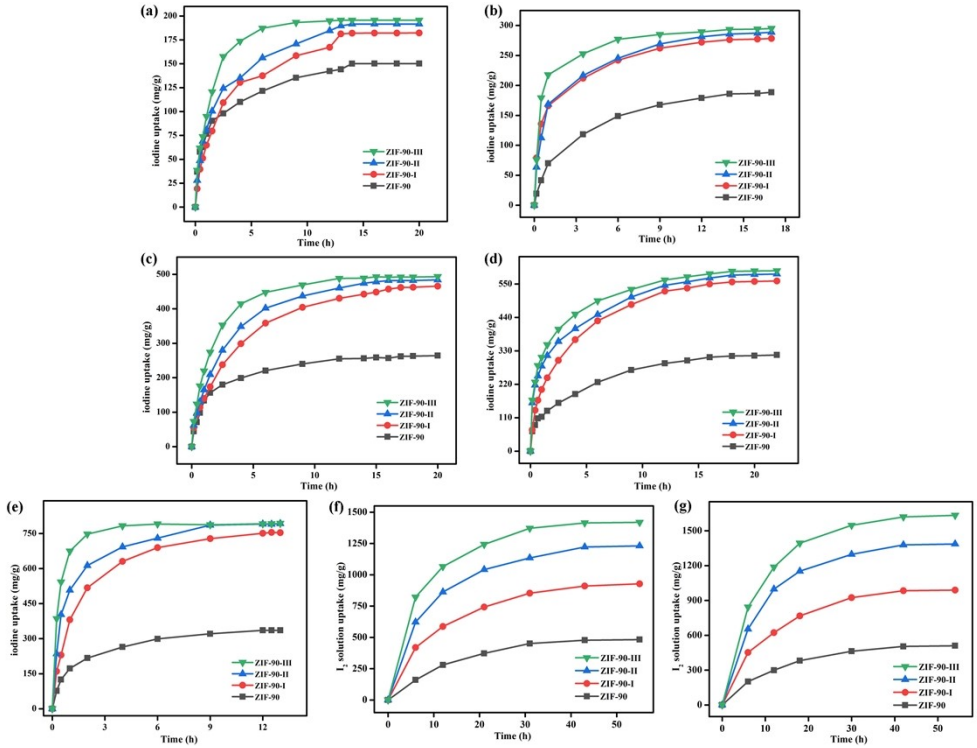

Fig. S33 Iodine adsorption plots of **ZIF-90** and **ZIF-90-I**–**ZIF-90-III** in iodine/cyclohexane solutions with different concentrations and volumes at room temperature.

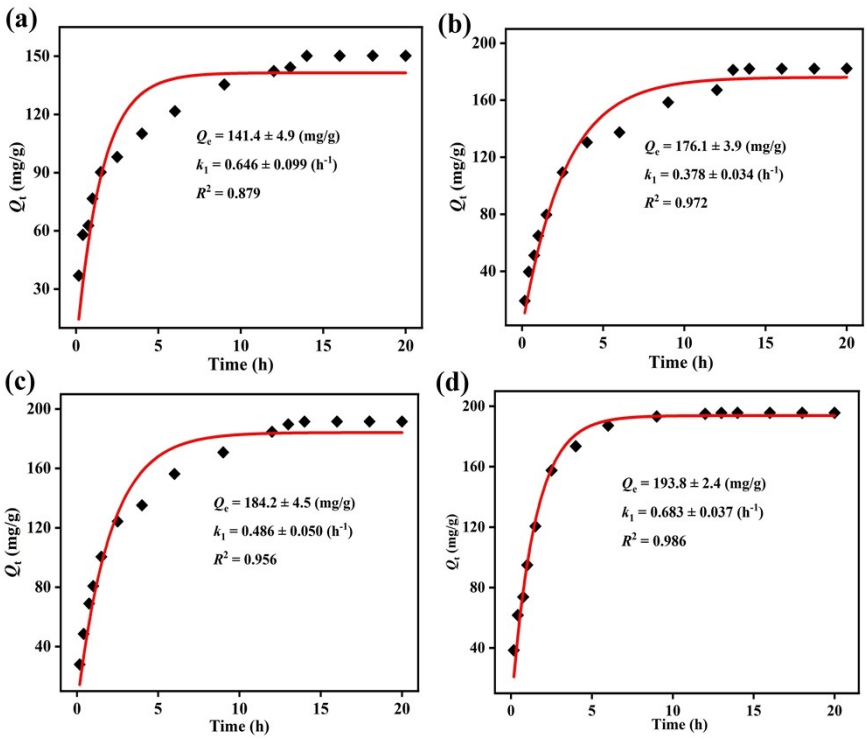

Fig. S34 The pseudo-first kinetic models for iodine adsorption kinetics of (a) **ZIF-90**, (b) **ZIF-90-I**, (c) **ZIF-90-II** and (d) **ZIF-90-III** in 5 mL of 200 mg/L iodine/cyclohexane solution.

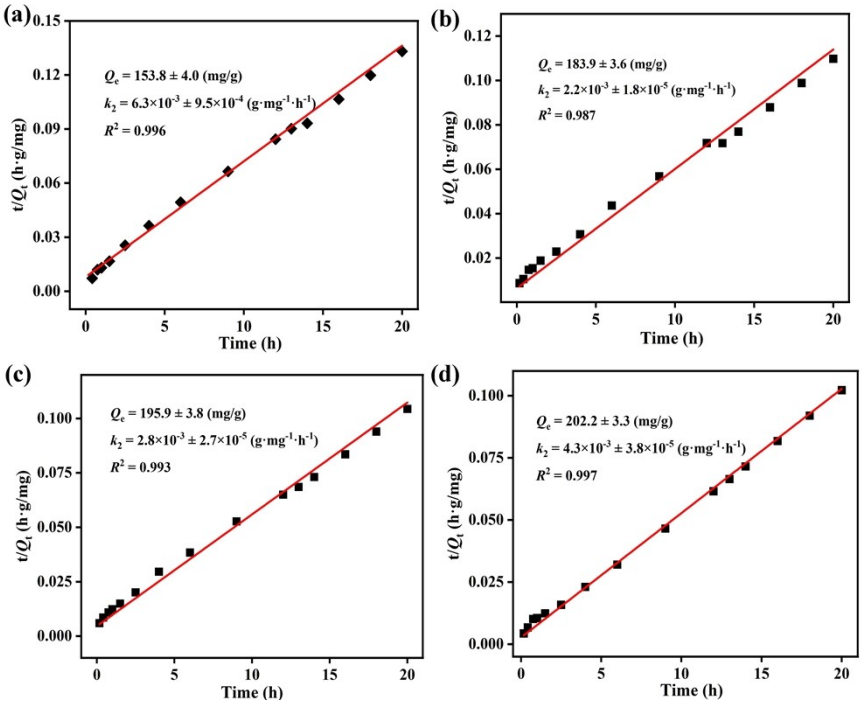

Fig. S35 The pseudo-second kinetic models for iodine adsorption kinetics of (a) **ZIF-90**, (b) **ZIF-90-I**, (c) **ZIF-90-II** and (d) **ZIF-90-III** in 5 mL of 200 mg/L iodine/cyclohexane solution.

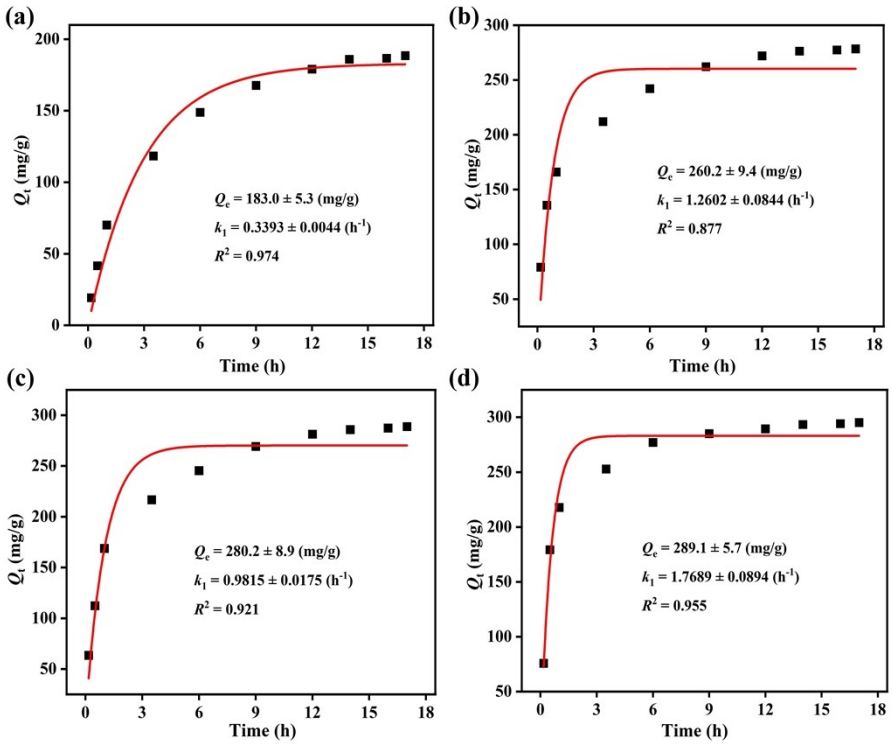

Fig. S36 The pseudo-first kinetic models for iodine adsorption kinetics of (a) **ZIF-90**, (b) **ZIF-90-I**, (c) **ZIF-90-II** and (d) **ZIF-90-III** in 5 mL of 300 mg/L iodine/cyclohexane solution.

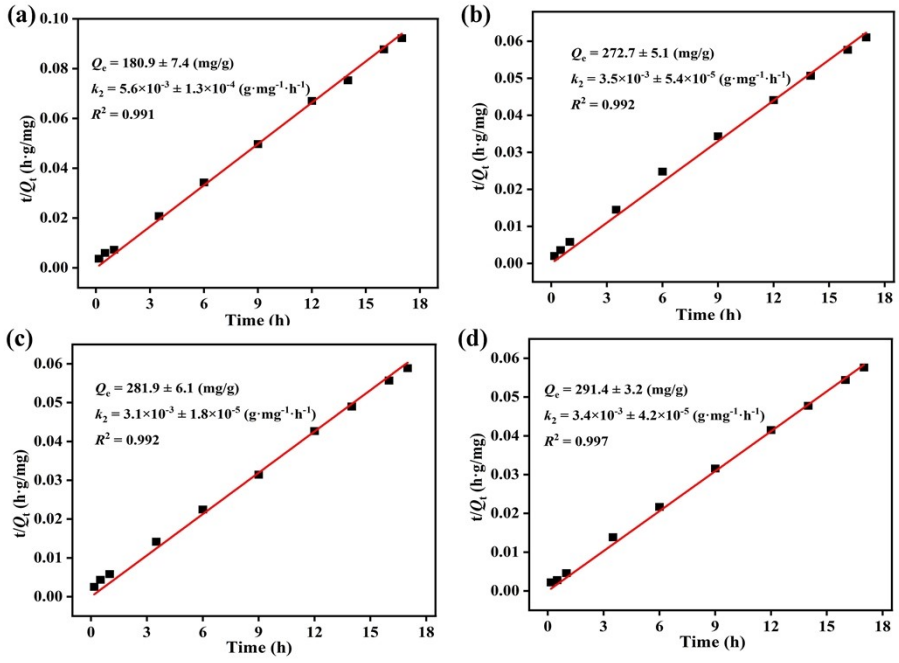

Fig. S37 The pseudo-second kinetic models for iodine adsorption kinetics of (a) **ZIF-90**, (b) **ZIF-90-I**, (c) **ZIF-90-II** and (d) **ZIF-90-III** in 5 mL of 300 mg/L iodine/cyclohexane solution.

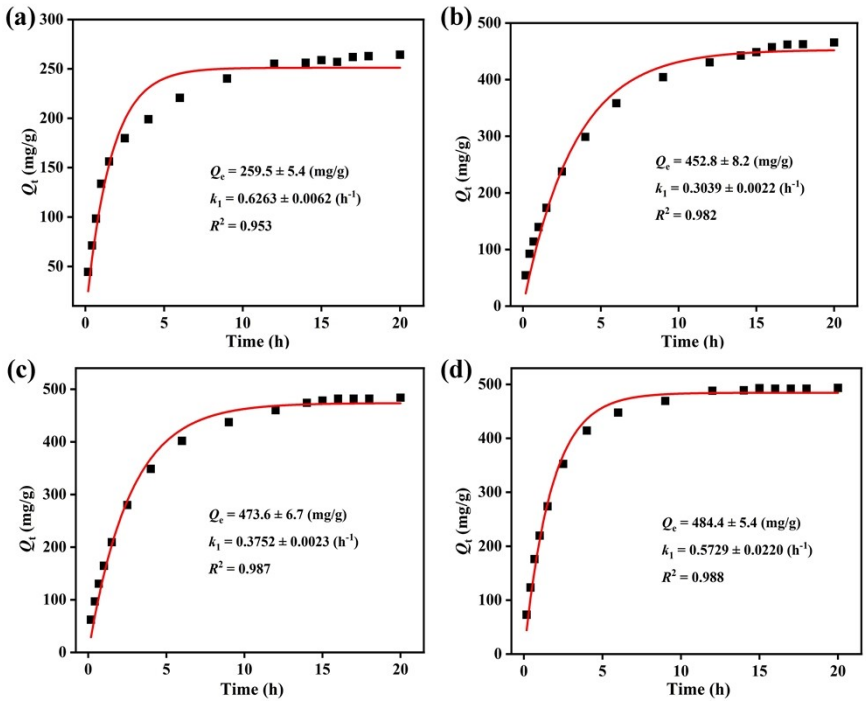

Fig. S38 The pseudo-first kinetic models for iodine adsorption kinetics of (a) **ZIF-90**, (b) **ZIF-90-I**, (c) **ZIF-90-II** and (d) **ZIF-90-III** in 5 mL of 500 mg/L iodine/cyclohexane solution.

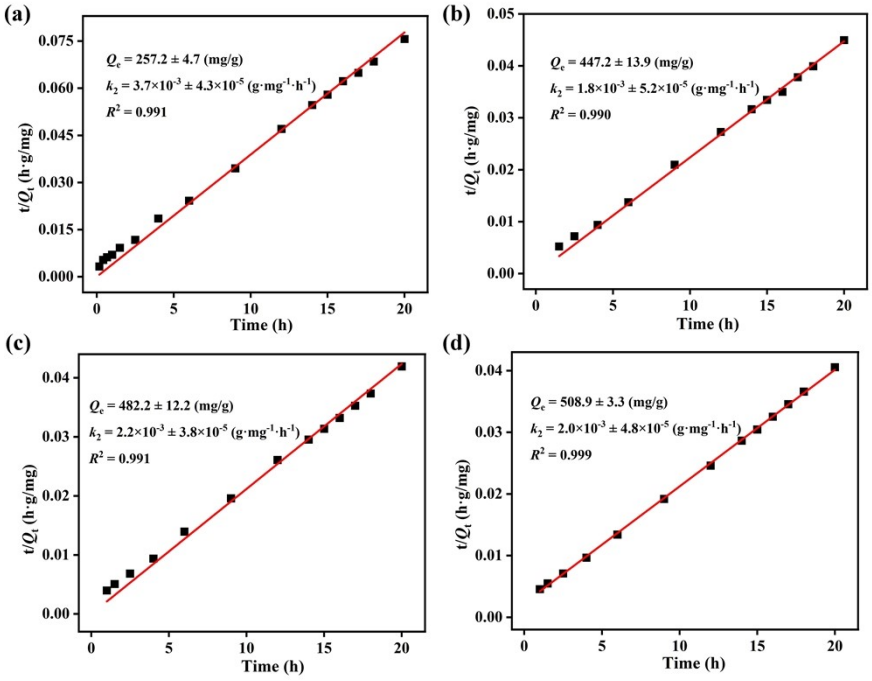

Fig. S39 The pseudo-second kinetic models for iodine adsorption kinetics of (a) **ZIF-90**, (b) **ZIF-90-I**, (c) **ZIF-90-II** and (d) **ZIF-90-III** in 5 mL of 500 mg/L iodine/cyclohexane solution.

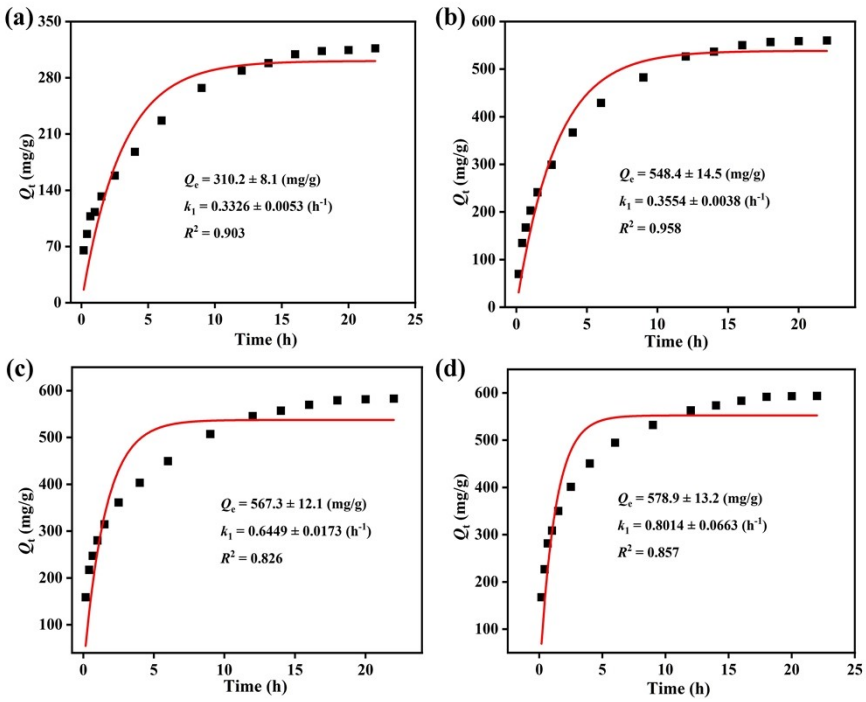

Fig. S40 The pseudo-first kinetic models for iodine adsorption kinetics of (a) **ZIF-90**, (b) **ZIF-90-I**, (c) **ZIF-90-II** and (d) **ZIF-90-III** in 5 mL of 600 mg/L iodine/cyclohexane solution.

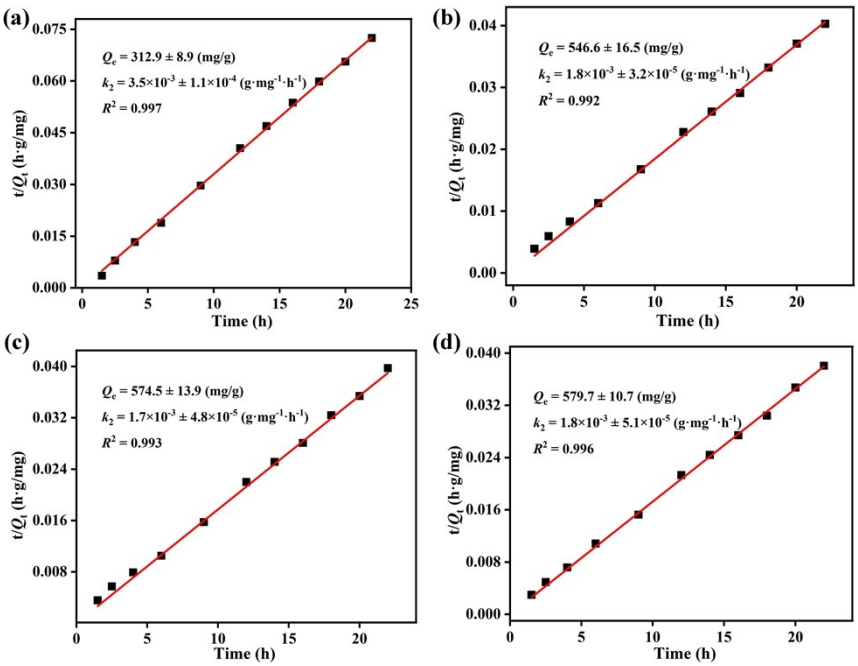

Fig. S41 The pseudo-second kinetic models for iodine adsorption kinetics of (a) **ZIF-90**, (b) **ZIF-90-I**, (c) **ZIF-90-II** and (d) **ZIF-90-III** in 5 mL of 600 mg/L iodine/cyclohexane solution.

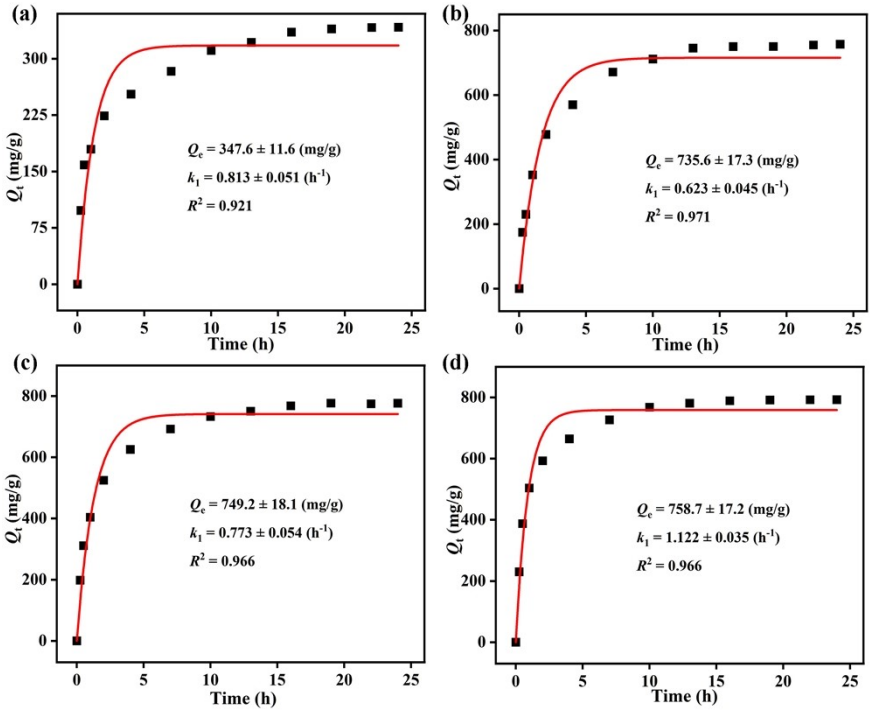

Fig. S42 The pseudo-first kinetic models for iodine adsorption kinetics of (a) **ZIF-90**, (b) **ZIF-90-I**, (c) **ZIF-90-II** and (d) **ZIF-90-III** in 5 mL of 800 mg/L iodine/cyclohexane solution.

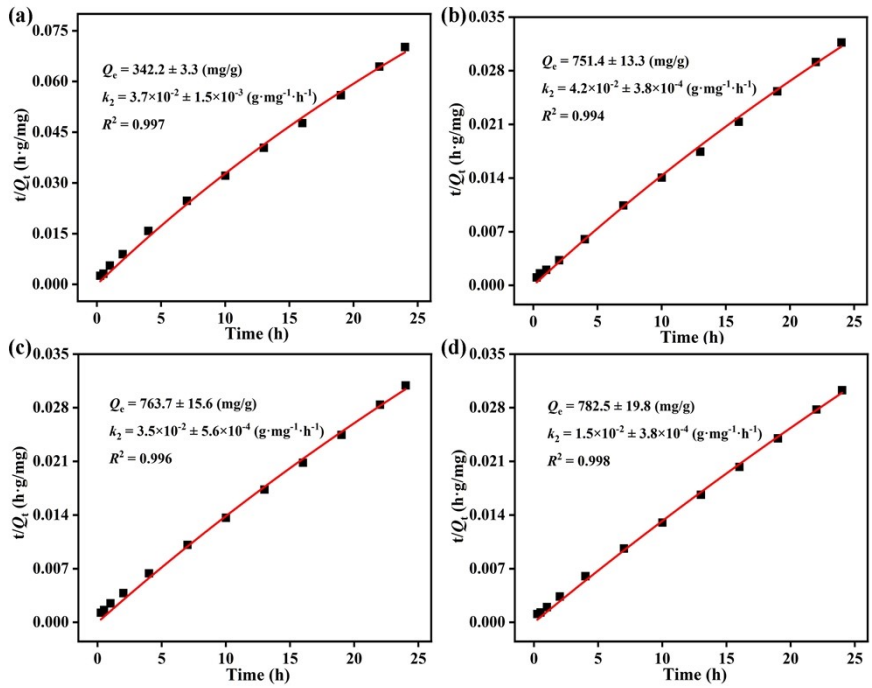

Fig. S43 The pseudo-second kinetic models for iodine adsorption kinetics of (a) **ZIF-90**, (b) **ZIF-90-I**, (c) **ZIF-90-II** and (d) **ZIF-90-III** in 5 mL of 800 mg/L iodine/cyclohexane solution.

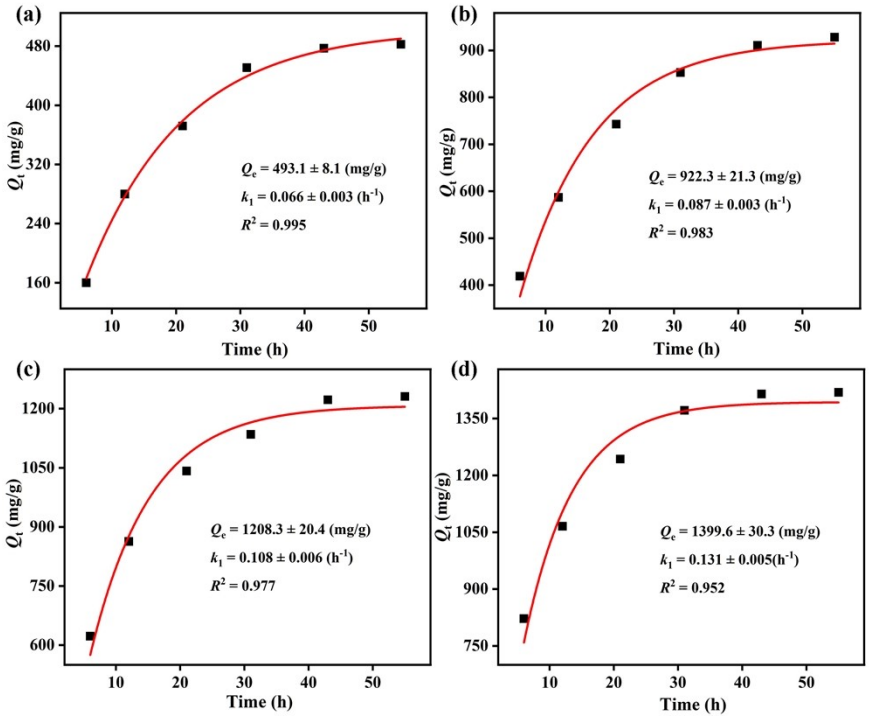

Fig. S44 The pseudo-first kinetic models for iodine adsorption kinetics of (a) **ZIF-90**, (b) **ZIF-90-I**, (c) **ZIF-90-II** and (d) **ZIF-90-III** in 15 mL of 500 mg/L iodine/cyclohexane solution.

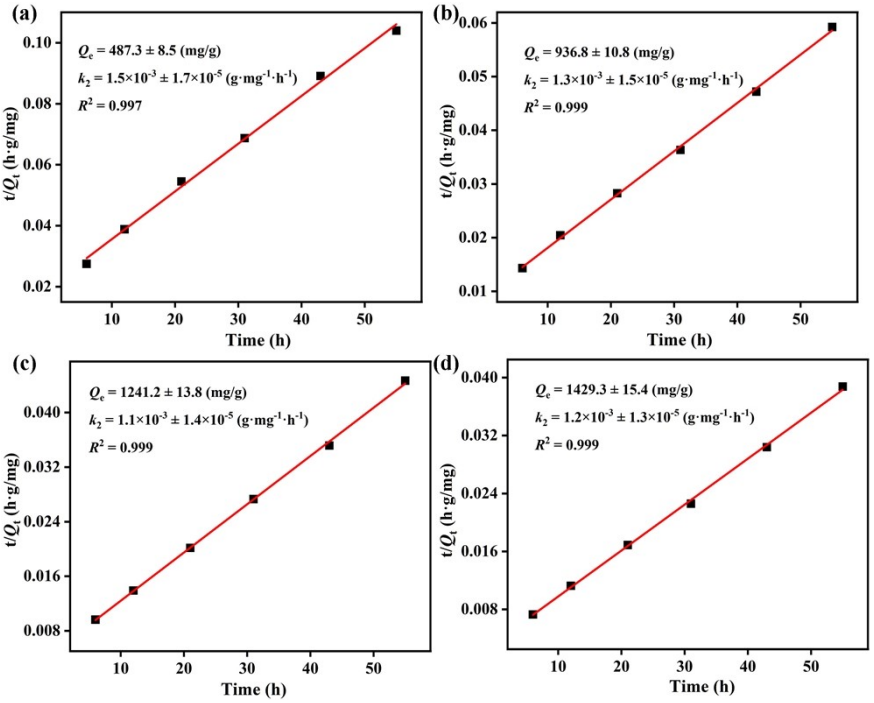

Fig. S45 The pseudo-second kinetic models for iodine adsorption kinetics of (a) **ZIF-90**, (b) **ZIF-90-I**, (c) **ZIF-90-II** and (d) **ZIF-90-III** in 15 mL of 500 mg/L iodine/cyclohexane solution.

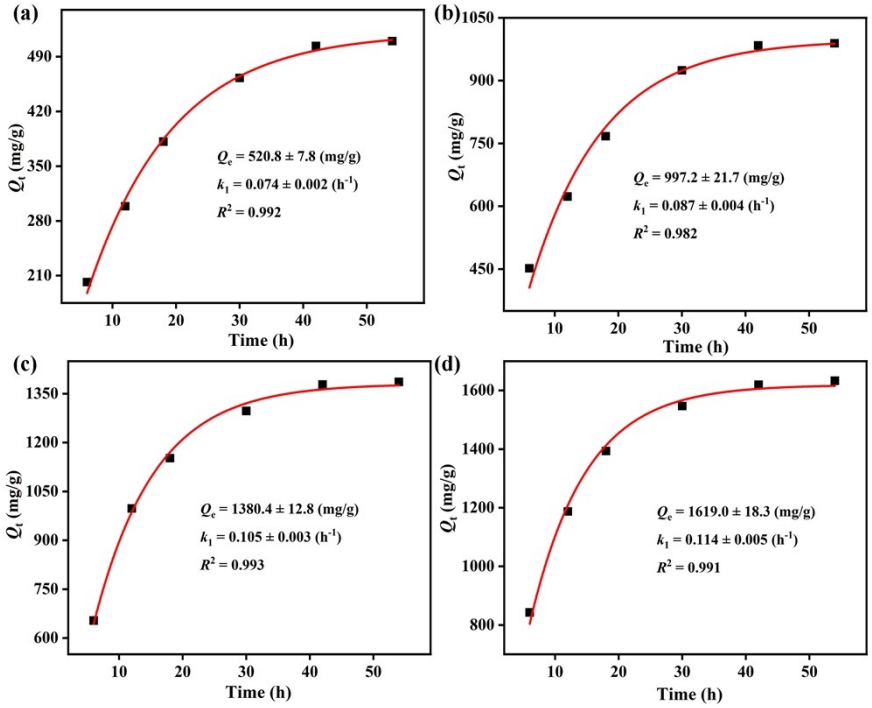

Fig. S46 The pseudo-first kinetic models for iodine adsorption kinetics of (a) **ZIF-90**, (b) **ZIF-90-I**, (c) **ZIF-90-II** and (d) **ZIF-90-III** in 15 mL of 700 mg/L iodine/cyclohexane solution.

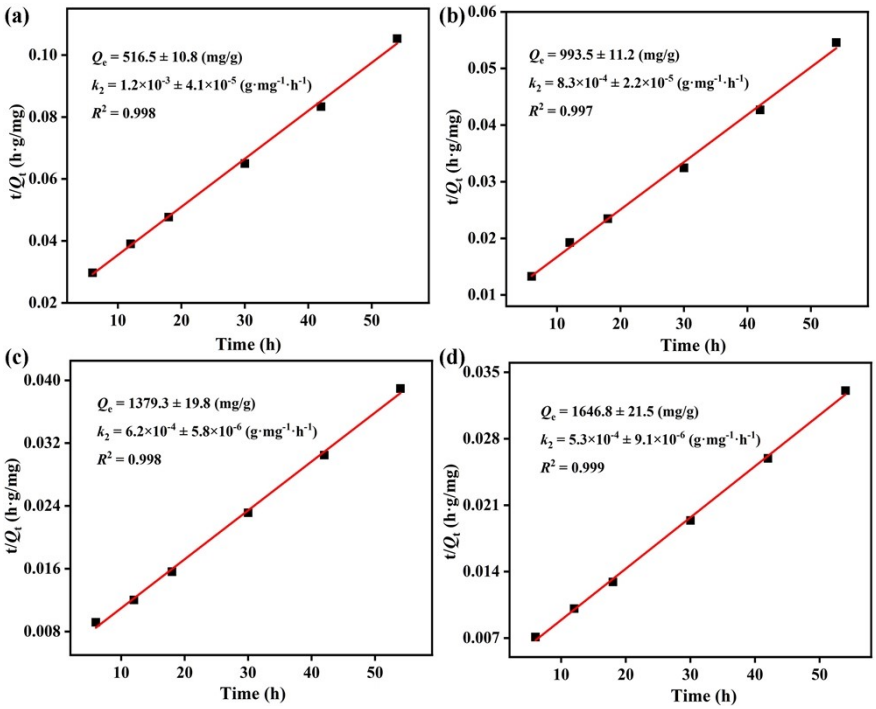

Fig. S47 The pseudo-second kinetic models for iodine adsorption kinetics of (a) **ZIF-90**, (b) **ZIF-90-I**, (c) **ZIF-90-II** and (d) **ZIF-90-III** in 15 mL of 700 mg/L iodine/cyclohexane solution.

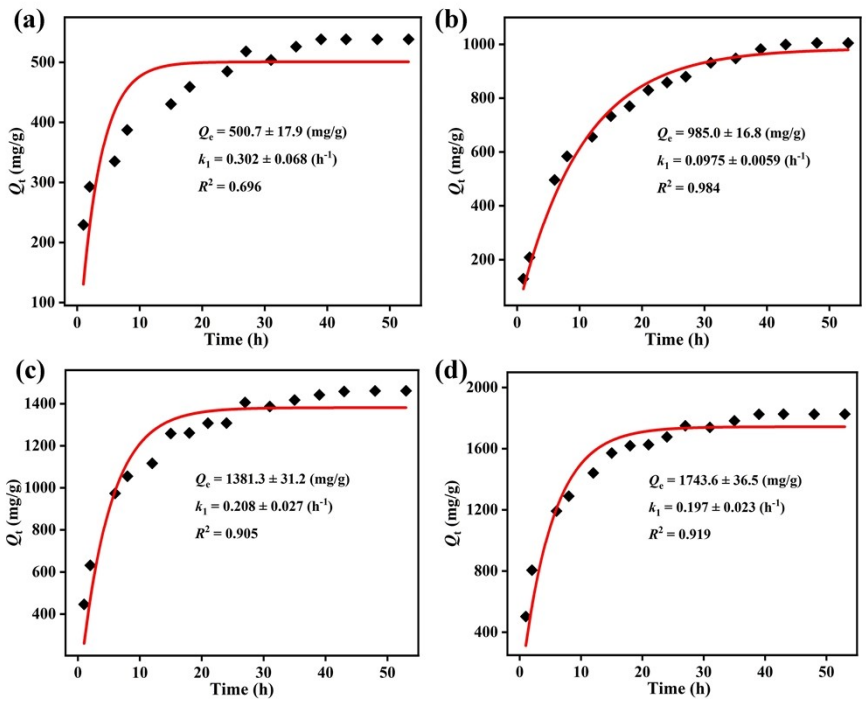

Fig. S48 The pseudo-first kinetic models for iodine adsorption kinetics of (a) **ZIF-90**, (b) **ZIF-90-I**, (c) **ZIF-90-II** and (d) **ZIF-90-III** in 15 mL of 1000 mg/L iodine/cyclohexane solution.

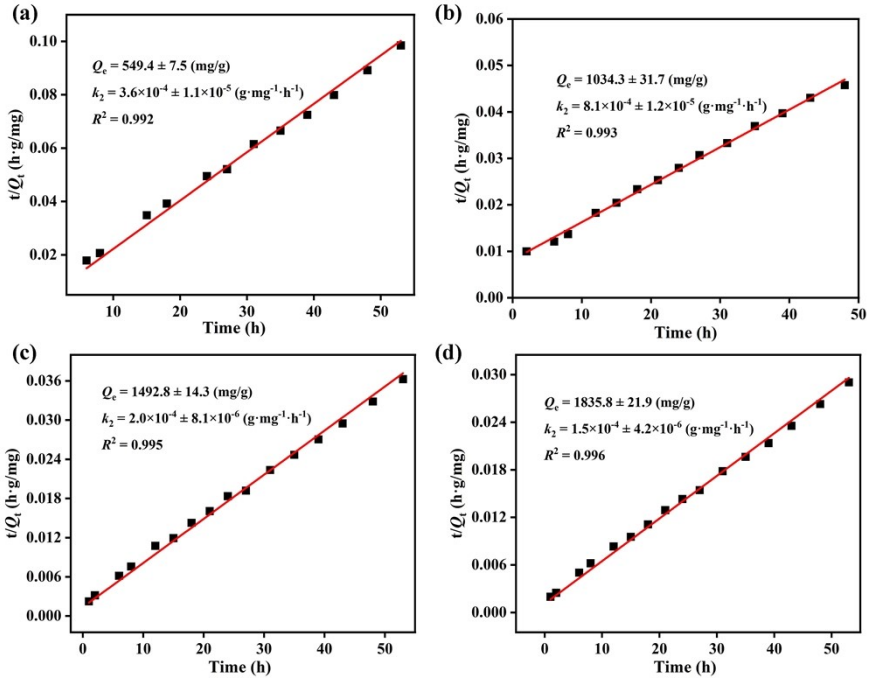

Fig. S49 The pseudo-second kinetic models for iodine adsorption kinetics of (a) **ZIF-90**, (b) **ZIF-90-I**, (c) **ZIF-90-II** and (d) **ZIF-90-III** in 15 mL of 1000 mg/L iodine/cyclohexane solution.

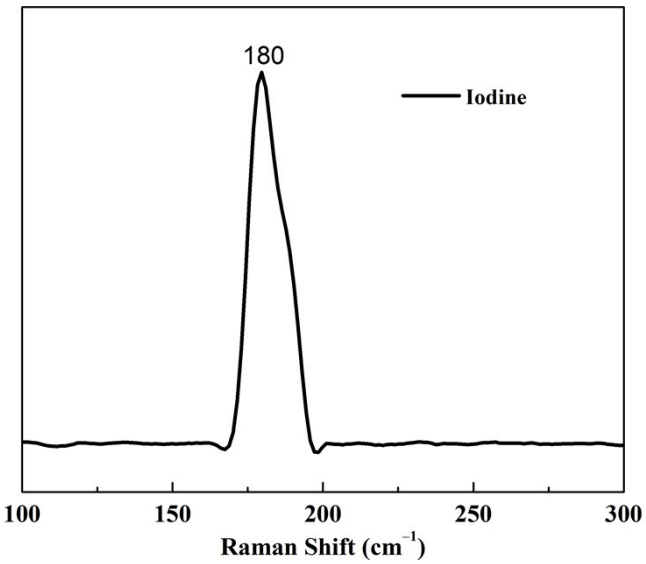

Fig. S50 Raman spectrum of pure I_2.

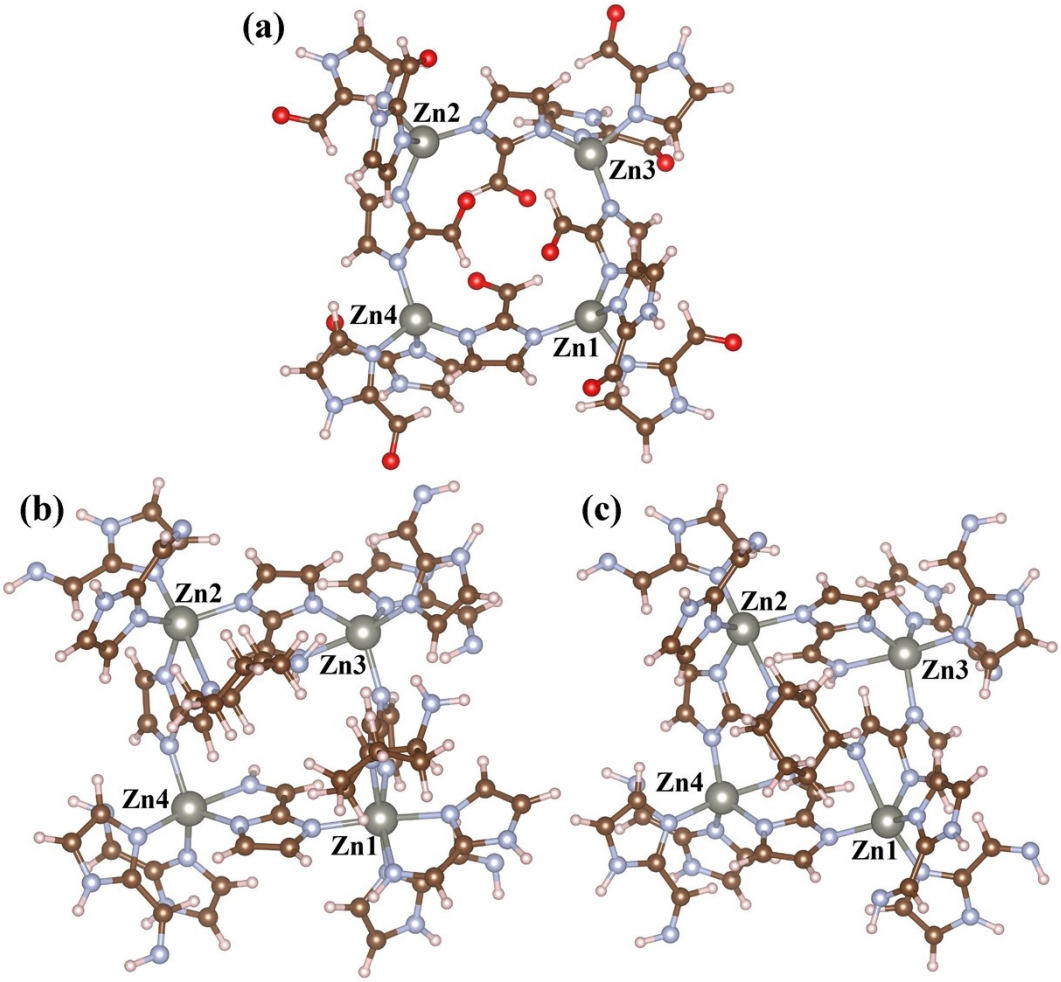

Fig. S51 Optimized geometries of the clusters for (a) **ZIF-90**, (b) **ZIF-90-mono** and (c) **ZIF-90-bis** (Zn: gray, O: red, C: brown, N: blue, and H: light pink).

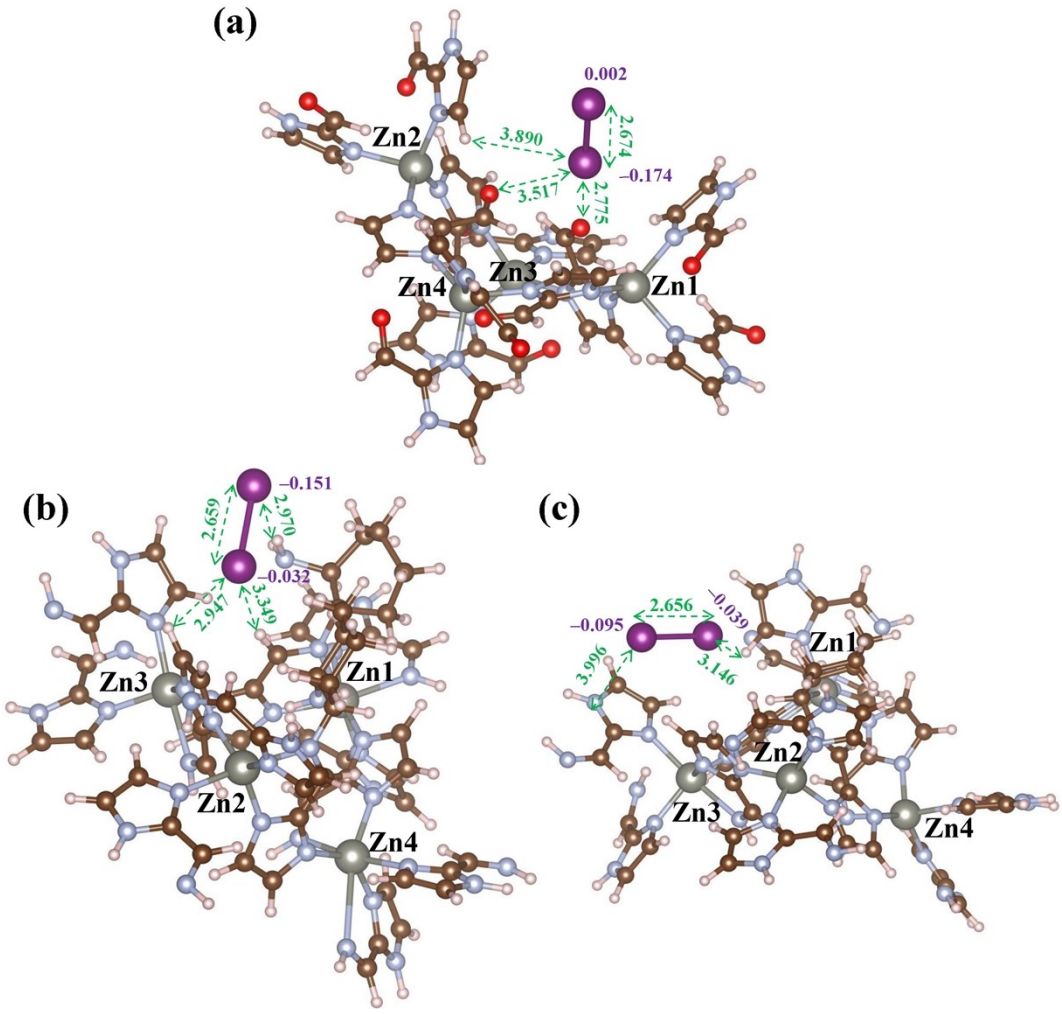

Fig. S52 Optimized geometries of composites with an iodine molecule and the cluster of (a) **ZIF-90**, (b) **ZIF-90-mono** and (c) **ZIF-90-bis**, respectively. The purple texts are the Mulliken charges (*e*) of iodine atoms. The green texts are the distances (Å) between two atoms labeled by the related green arrow. (Zn: gray, O: red, C: brown, N: blue, and H: light pink).

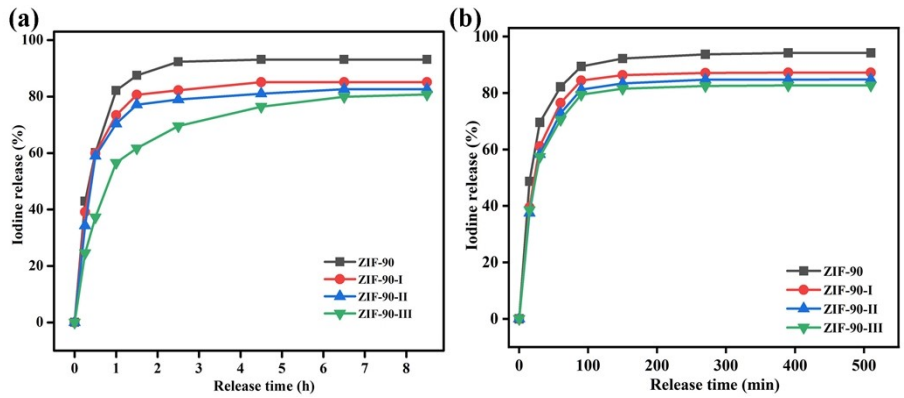

Fig. S53 Iodine release experiments of iodine-loaded **ZIF-90** and **ZIF-90-I**–**ZIF-90-III** with iodine from (a) iodine vapour, (b) iodine/cyclohexane solution at 120 °C.

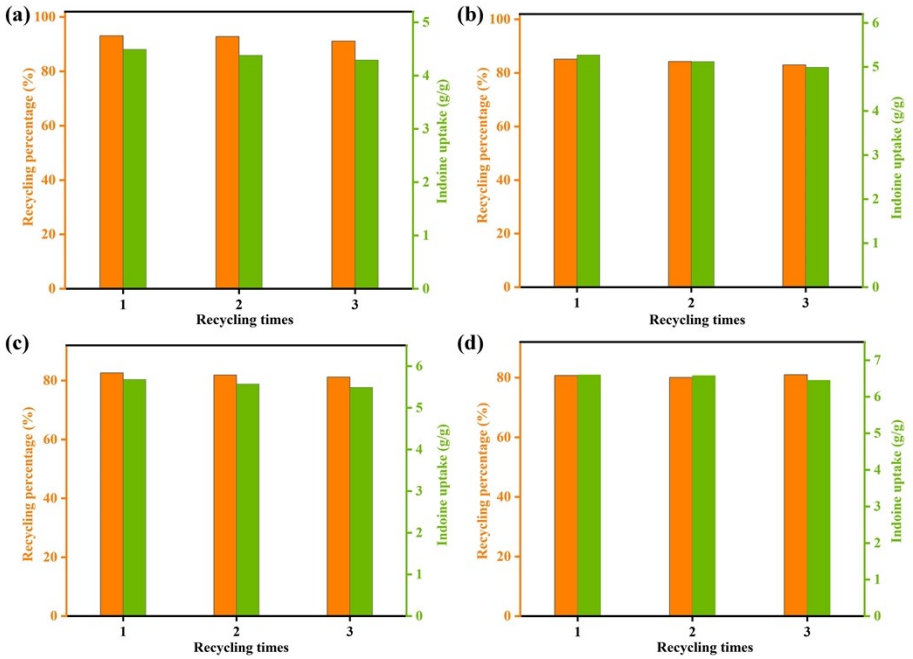

Fig. S54 Recycling tests of (a) **ZIF-90**, (b) **ZIF-90-I**, (c) **ZIF-90-II** and (d) **ZIF-90-III** for iodine vapour.

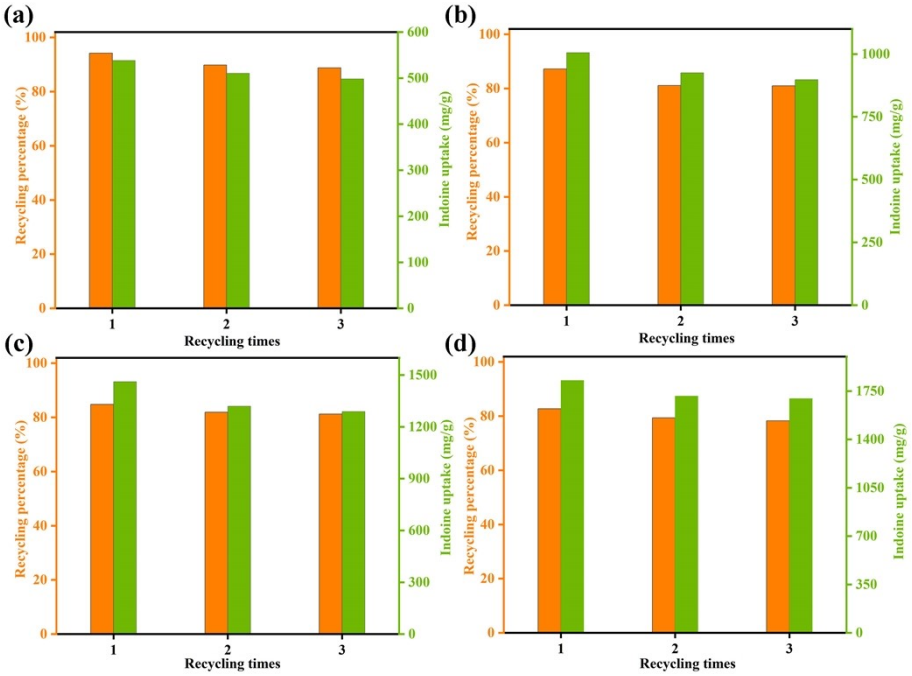

Fig. S55 Recycling tests of (a) **ZIF-90**, (b) **ZIF-90-I**, (c) **ZIF-90-II** and (d) **ZIF-90-III** for iodine/cyclohexane solution.

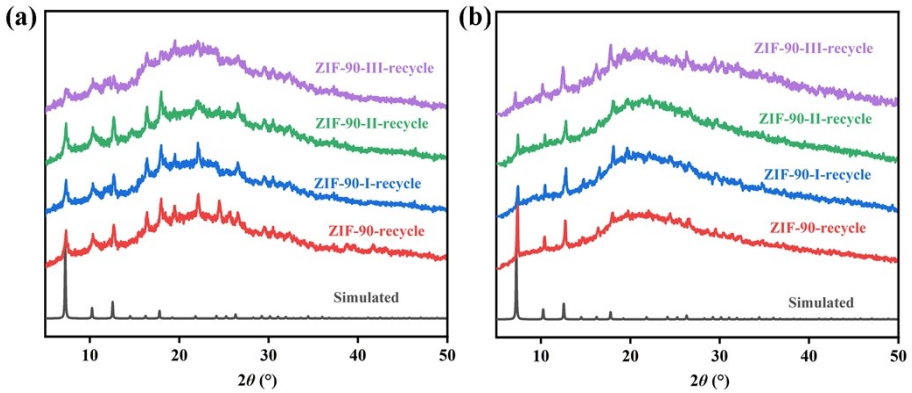

Fig. S56 PXRD patterns of recovered **ZIF-90** and **ZIF-90-I**–**ZIF-90-III** after iodine release experiments (iodine came from (a) iodine vapour and (b) iodine/cyclohexane solution).

Table S1 Experimental and calculated *m*/*z* values of the isotopic envelopes for digested **ZIF-90**

Chemistry Formula	Experimental *m*/*z* value	Calculated *m*/*z* value
$[H(L^1)]^+$	97.04	97.04
$[(HCOOH)(H_3O)]^+$	111.05	111.03
$[Zn(L^1)]^+$	160.90	160.95
$[Zn(L^1)(HCOOH)]^+$	204.90	204.96
$Zn[H(L^1)_2]^+$	254.90	254.99

Table S2 Experimental and calculated *m*/*z* values of the isotopic envelopes for digested **ZIF-90-I**

Chemistry Formula	Experimental *m* / *z* value	Calculated *m* / *z* value
$[H(L^1)]^+$	97.04	97.04
$[(HCOOH)(H_3O)]^+$	111.05	111.03
$[(HCOOH)_2(CH_3OH)H]^+$	125.10	125.10
$[Zn(L^1)]^+$	160.90	160.95
$[Zn(L^1)(H_2O)]^+$	179.00	178.96
$[Zn(L^1)(HCOOH)]^+$	204.90	204.96
$[Zn(L^1)(HCOOH)(H_2O)]^+$	223.04	222.97
$[Zn(L^2)]^+$	255.06	255.06
$[Zn(L^2)(H_2O)]^+$	273.06	273.07
$[Zn(L^2)(HCOOH)]^+$	301.06	301.06
$[Zn(L^3)]^+$	333.09	333.08

Table S3 Experimental and calculated *m*/*z* values of the isotopic envelopes for digested **ZIF-90-II**

Chemistry Formula	Experimental *m*/*z* value	Calculated *m*/*z* value
$[H(L^1)]^+$	97.04	97.04
$[(HCOOH)(H_3O)]^+$	111.05	111.03
$[(HCOOH)_2(CH_3OH)H]^+$	125.10	125.10
$[Zn(L^1)]^+$	160.90	160.95
$[Zn(L^1)(HCOOH)]^+$	204.90	204.96
$[Zn(L^2)]^+$	255.06	255.06
$[Zn(L^2)(H_2O)]^+$	273.06	273.07
$[Zn(L^2)(HCOOH)]^+$	301.06	301.06
$[Zn(L^3)]^+$	333.09	333.08

Table S4 Experimental and calculated *m*/*z* values of the isotopic envelopes for digested **ZIF-90-III**

Chemistry Formula	Experimental *m*/*z* value	Calculated *m*/*z* value
$[H(L^1)]^+$	97.04	97.04
$[(HCOOH)(H_3O)]^+$	111.05	111.03
$[(HCOOH)_2(CH_3OH)H]^+$	125.10	125.10
$[Zn(L^1)]^+$	160.90	160.95
$[Zn(L^1)(H_2O)]^+$	179.00	178.96
$[Zn(L^1)(HCOOH)]^+$	204.90	204.96
$[Zn(L^2)]^+$	255.06	255.06
$[Zn(L^2)(H_2O)]^+$	273.06	273.07
$[Zn(L^2)(HCOOH)]^+$	301.06	301.06
$[Zn(L^3)]^+$	333.09	333.08

Table S5 Summary of iodine adsorption in MOFs via vapor diffusion

MOF	Iodine uptake (g/g)	Ref.
IL@PCN-333(Al)	7.35	1
ZIF-90-III	6.60	this work
ZIF-90-II	5.68	this work
ZIF-90-I	5.27	this work
ZIF-90	4.49	this work
PCN-333(Al)	4.42	1
Cu@MIL-101	3.42	2
UPC-158-HCl	2.92	3
$[Zr_6O_4(OH)_4(peb)_6]$	2.79	4
UPC-158-HBr	2.75	3
UPC-158-HI	2.59	3
$Ti_{16}Pb_5O_{16}(C_6H_5CO_2)_2(OCH_3)_{40}$	2.2	5
UPC-158-HF	2.19	3
MOF-808	2.18	6
Zn_2(tptc)(apy)	2.16	7
$[(Cu_2I_2)$(3-TPPM)$](DMF)_3(H_2O)_{1.3}$	1.90	8
UPC-158	1.78	3
Cu-BTC	1.75	9
$[(ZnI_2)_3(TPT)_2]$	1.73	10
MFM-300(Sc)	1.54	11
NU-1000	1.45	6
MOF-808@PVDF	1.42	12
MFM-300(Fe)	1.29	11
ZIF-8	1.25	13

Th-SINAP-1	1.24	14
UiO-67-$(NH_2)_2$	1.211	15
ZrTBPA-ns	1.20	16
MFM-300(In)	1.16	11
DUT-68(Zr)	1.081	17
JNU-200	1.08	18
UiO-67-NH_2	1.071	15
ZrTBPA-tb	0.95	16
MFM-300(Al)	0.94	11
MOF-867	0.88	6
AlOC-155	0.86	19
DUT-67(Zr)	0.843	17
AlOC-151	0.73	19
UIO-66	0.66	6
UiO-67-CH_2NH_2	0.660	15
UiO-66-NH_2	0.565	15
UIO-67	0.53	6
Ca(tcpb)	0.43	20
UiO-66-$(OH)_2$	0.388	15
HKUST-1@PES	0.376	21
HKUST-1@PEI	0.348	21
UiO-66-Napht	0.323	15
UiO-68-NH_2	0.300	15
UiO-66-NO_2	0.290	15
UiO-66-Br	0.277	15
Ca(sdb)	0.226	20
UiO-66-CH_3	0.235	15
HKUST-1@PVDF	0.225	21

Table S6 The maximum iodine vapor adsorption (mg/g) of **ZIF-90** and **ZIF-90-I**–**ZIF-90-III** at different temperatures

Temperature (°C)	**ZIF-90**	**ZIF-90-I**	**ZIF-90-II**	**ZIF-90-III**
40	2810	3749	4001	4300
50	3330	3887	4260	4634
60	3350	3974	4410	5210
75	4490	5270	5680	6600
90	4551	5380	5604	6342

Table S7 Adsorption kinetic parameters of iodine vapor adsorption by **ZIF-90** at different temperatures

Temperature (°C)	$Q_{e,exp}$ (mg/g)	Pseudo-first-order			Pseudo-second-order		
		k_1 (h^{-1})	$Q_{e,cal}$ (mg/g)	R^2	k_2 ($g \cdot mg^{-1} \cdot h^{-1}$)	$Q_{e,cal}$ (mg/g)	R^2
40	2810	0.0047	2905.8±21.3	0.971	4.2×10^{-7}	2775.1±82.9	0.759
50	3330	0.0168	3481.4±56.7	0.995	9.5×10^{-7}	3405.1±34.6	0.939
60	3350	0.0401	3445.6±91.3	0.979	1.2×10^{-5}	3401.1±44.6	0.864
75	4490	0.0558	4575.8±91.3	0.991	2.1×10^{-5}	4878.1±134.6	0.945
90	4551	0.0797	4677.9±92.1	0.995	2.3×10^{-5}	4821.5±125.6	0.907

Table S8 Adsorption kinetic parameters of iodine vapor adsorption by **ZIF-90-I** at different temperatures

Temperature (°C)	$Q_{e,exp}$ (mg/g)	Pseudo-first-order			Pseudo-second-order		
		k_1 (h^{-1})	$Q_{e,cal}$ (mg/g)	R^2	k_2 ($g \cdot mg^{-1} \cdot h^{-1}$)	$Q_{e,cal}$ (mg/g)	R^2
40	3749	0.0101	3813.4±113.3	0.975	3.9×10^{-6}	3824.6±78.6	0.995
50	3887	0.0261	3981.4±53.3	0.992	6.2×10^{-6}	3898.1±23.1	0.998
60	3974	0.1002	3849.9±109.1	0.964	1.5×10^{-5}	3850.2±104.7	0.989
75	5270	0.1130	5175.8±85.9	0.984	2.4×10^{-5}	5359.1±91.4	0.994
90	5380	0.2539	5389.7±100.1	0.991	3.2×10^{-5}	5341.1±87.9	0.997

Table S9 Adsorption kinetic parameters of iodine vapor adsorption by **ZIF-90-II** at different temperatures

Temperature (°C)	$Q_{e,exp}$ (mg/g)	Pseudo-first-order			Pseudo-second-order		
		k_1 (h^{-1})	$Q_{e,cal}$ (mg/g)	R^2	k_2 ($g \cdot mg^{-1} \cdot h^{-1}$)	$Q_{e,cal}$ (mg/g)	R^2
40	4001	0.0092	4001.0±132.5	0.974	5.0×10^{-6}	4001.1±34.6	0.995
50	4260	0.0292	4324.4±45.1	0.995	9.6×10^{-6}	4316.9±38.6	0.996
60	4410	0.0782	4303.8±90.0	0.985	1.8×10^{-5}	4298.6±115.0	0.991
75	5680	0.1350	5465.7±79.1	0.985	2.6×10^{-5}	5788.0±81.1	0.996
90	5604	0.2711	5536.3±132.1	0.985	3.5×10^{-5}	5553.3±91.6	0.997

Table S10 Adsorption kinetic parameters of iodine vapor adsorption by **ZIF-90-III** at different temperatures

Temperature (°C)	$Q_{e,exp}$ (mg/g)	Pseudo-first-order			Pseudo-second-order		
		k_1 (h^{-1})	$Q_{e,cal}$ (mg/g)	R^2	k_2 ($g \cdot mg^{-1} \cdot h^{-1}$)	$Q_{e,cal}$ (mg/g)	R^2
40	4300	0.0113	4321.8±91.4	0.985	5.6×10^{-6}	4401.1±50.7	0.991
50	4634	0.0374	4635.1±23.6	0.998	1.2×10^{-5}	4644.1±34.6	0.998
60	5210	0.1070	5175.3±160.6	0.951	1.9×10^{-5}	5097.9±130.6	0.998
75	6600	0.1360	6325.2±89.1	0.986	2.3×10^{-5}	6707.9±54.5	0.997
90	6342	0.3068	6219.5±111.4	0.990	3.8×10^{-5}	6298.4±113.3	0.998

Table S11 The iodine equilibrium amount (mg/g) of **ZIF-90** and **ZIF-90-I**–**ZIF-90-III** in iodine/cyclohexane solution with different concentrations

C_0 (mg/L) × V (mL)	**ZIF-90**	**ZIF-90-I**	**ZIF-90-II**	**ZIF-90-III**
200 × 5	150	182	192	196
300 × 5	188	278	289	295
500 × 5	264	466	484	493
600 × 5	317	560	583	594
800 × 5	342	757	776	792
500 × 15	483	928	1231	1419
700 × 15	510	989	1386	1633
1000 × 15	538	1005	1461	1826

Table S12 Summary of iodine adsorption in MOFs via solution-based processes

MOF	Iodine uptake (g/g)	Ref.
IL@PCN-333(Al)	3.4	1
$Ti_{16}Pb_5O_{16}(C_6H_5CO_2)_2(OCH_3)_{40}$	3.1	5
Ag@MIL-101	2.14	22
ZIF-90-III	1.826	this work
ZIF-90-II	1.461	this work
TMU-15	1.30	23
TMU-16-NH_2	1.28	24
AgNPs@UiO-66	1.26	25
UIO-66	1.25	6

$[WS_4Cu_4(\mu\text{-}CN)_2(bpea)_2]\cdot 1.5DMF$	1.106	26
$[Cu_8I_6(CN)_2(PPh_3)_4]_n$	1.104	27
IFMC-15	1.10	28
ZIF-90-I	1.005	this work
$[Cd(pbica)_2]\cdot 1.5DMF\cdot 2CH_3OH$	1.00	29
BOF-1	0.93	30
MBM	0.88	31
Ag-MSHC-6	0.77	32
$[Co(ebic)_2]_n$	0.75	33
$[Zn(ebic)_2]_n$	0.74	33
$Cu(H_2L^5)$	0.66	34
AlOC-83	0.555	37
ZIF-90	0.538	this work
$[Cu_4Cl_3(TPVS)_4(H_2O)_2]\cdot Cl_5\cdot DMF\cdot MeOH$	0.485	35
Th-SINAP-8	0.473	36
$[Cu^{II}(btz)]_n$	0.47	38
$[Zn_7(L^4)_3]_n[Zn_5(L^4)_3]_n$	0.46	39
Cu/MIL-101	0.432	2
$\{[Cu_6(pybz)_8(OH)_2]\cdot I_5^-\cdot I_7^-\}_n$	0.432	40
HKUST-1@PES	0.376	21
HKUST-1@PEI,	0.348	21
SCNU-Z4	0.332	41
MIL-101-NH_2(Al)	0.31	42
JLU-Liu32	0.29	45
$[Cd(2\text{-}NH_2bdc)(4\text{-}bpmh)]_n$	0.28	43
$[Zn_3(L^2)_2(\mu_2\text{-}OH)_2]_n$	0.28	44
$[Zn_3(L^3)_2(\mu_2\text{-}OH)_2]_n$	0.26	44
JLU-Liu31	0.25	45
$Ag_2O\text{-}Ag_2O_3$@ZIF-8	0.23	46
HKUST-1@ PVDF	0.225	21
TMU-16	0.22	24
$[Zn_3(BTC)_2(TIB)_2]_n$	0.21	47
$\{[WS_4Cu_4(4,4\text{-}bpy)_4][WS_4Cu_4I_4(4,4\text{-}bpy)_2]\}$	0.20	48
$[Cd(L^1)_2(ClO_4)_2]$	0.19	49
MIL-53-NH_2(Al)	0.18	42
Cu_2TMBD	0.18	50
JLU-Liu14	0.16	51
$[Cd_3(BTC)_2(TIB)_2]_n$	0.16	47
$[Cd(bdc)(4\text{-}bpmh)]_n$	0.15	43
[DMA][In(TDC)$_2$]	0.10	52
$\{[Zn_2(a\text{-}bptc)(H_2O)_4]\cdot(pra)\}_n$	0.085	53

Table S13 Adsorption kinetic parameters of iodine adsorption by **ZIF-90** from iodine/cyclohexane solution with different concentrations

C_0 (mg/L) × V (mL)	$Q_{e,exp}$ (mg/g)	Pseudo-first-order			Pseudo-second-order		
		k_1 (h^{-1})	$Q_{e,cal}$ (mg/g)	R^2	k_2 ($g \cdot mg^{-1} \cdot h^{-1}$)	$Q_{e,cal}$ (mg/g)	R^2
200 × 5	150	0.646	141.4±4.9	0.879	6.3×10^{-3}	153.8±4.0	0.996
300 × 5	188	0.3393	183.0±5.3	0.974	5.6×10^{-3}	180.9±7.4	0.991
500 × 5	264	0.6263	259.5±5.4	0.953	3.7×10^{-3}	257.2±4.7	0.991
600 × 5	317	0.3326	310.2±8.1	0.903	3.5×10^{-3}	312.9±8.9	0.997
800 × 5	342	0.813	347.6±11.6	0.921	3.7×10^{-2}	342.2±3.3	0.997
500 × 15	483	0.066	493.1±8.1	0.995	1.5×10^{-3}	487.3±8.5	0.997
700 × 15	510	0.074	520.8±7.8	0.992	1.2×10^{-3}	516.5±10.8	0.998
1000 × 15	538	0.302	500.7±17.9	0.696	3.6×10^{-4}	549.4±7.5	0.992

Table S14 Adsorption kinetic parameters of iodine adsorption by **ZIF-90-I** from iodine/cyclohexane solution with different concentrations

C_0 (mg/L) × V (mL)	$Q_{e,exp}$ (mg/g)	Pseudo-first-order			Pseudo-second-order		
		k_1 (h^{-1})	$Q_{e,cal}$ (mg/g)	R^2	k_2 ($g \cdot mg^{-1} \cdot h^{-1}$)	$Q_{e,cal}$ (mg/g)	R^2
200 × 5	182	0.378	176.1±3.9	0.972	2.2×10^{-3}	183.9±3.6	0.987
300 × 5	278	1.2602	260.2±9.4	0.877	3.5×10^{-3}	272.7±5.1	0.992
500 × 5	466	0.3039	452.8±8.2	0.982	1.8×10^{-3}	447.2±13.9	0.990
600 × 5	560	0.3554	548.4±14.5	0.958	1.8×10^{-3}	546.6±16.5	0.992
800 × 5	757	0.624	735.6±17.3	0.971	4.2×10^{-2}	751.4±13.3	0.994
500 × 15	928	0.087	922.3±21.3	0.983	1.3×10^{-3}	936.8±10.8	0.999
700 × 15	989	0.087	997.2±21.7	0.982	8.3×10^{-4}	993.5±11.2	0.997
1000 × 15	1005	0.0975	985.0±16.8	0.984	8.1×10^{-4}	1034.3±31.7	0.993

Table S15 Adsorption kinetic parameters of iodine adsorption by **ZIF-90-II** from iodine/cyclohexane solution with different concentrations

C_0 (mg/L) × V (mL)	$Q_{e,exp}$ (mg/g)	Pseudo-first-order			Pseudo-second-order		
		k_1 (h^{-1})	$Q_{e,cal}$ (mg/g)	R^2	k_2 ($g \cdot mg^{-1} \cdot h^{-1}$)	$Q_{e,cal}$ (mg/g)	R^2
200 × 5	192	0.486	184.2±4.5	0.956	2.8×10^{-3}	195.9±3.8	0.993
300 × 5	289	0.9815	280.2±8.9	0.921	3.1×10^{-3}	281.9±6.1	0.992
500 × 5	484	0.3752	473.6±6.7	0.987	2.2×10^{-3}	482.2±12.2	0.991
600 × 5	583	0.6449	567.3±12.1	0.826	1.7×10^{-3}	574.5±13.9	0.993
800 × 5	776	0.773	749.2±18.1	0.966	3.5×10^{-2}	763.7±15.6	0.996
500 × 15	1231	0.108	1208.3±20.4	0.977	1.1×10^{-3}	1241.2±13.8	0.999
700 × 15	1386	0.105	1380.4±12.8	0.993	6.2×10^{-4}	1379.3±19.8	0.998
1000 × 15	1461	0.208	1381.3±31.2	0.905	2.0×10^{-4}	1492.8±14.3	0.995

Table S16 Adsorption kinetic parameters of iodine adsorption by **ZIF-90-III** from iodine/cyclohexane solution with different concentrations

C_0 (mg/L) × V (mL)	$Q_{e,exp}$ (mg/g)	Pseudo-first-order			Pseudo-second-order		
		k_1 (h^{-1})	$Q_{e,cal}$ (mg/g)	R^2	k_2 ($g \cdot mg^{-1} \cdot h^{-1}$)	$Q_{e,cal}$ (mg/g)	R^2
200 × 5	196	0.683	193.8±2.4	0.986	4.3×10^{-3}	202.2±3.3	0.997
300 × 5	295	1.7689	289.1±5.7	0.955	3.4×10^{-3}	291.4±3.2	0.997
500 × 5	493	0.5729	484.4±5.4	0.988	2.0×10^{-3}	508.9±3.3	0.999
600 × 5	594	0.8014	578.9±13.2	0.857	1.8×10^{-3}	579.7±10.7	0.996
800 × 5	792	1.122	758.7±17.2	0.966	1.5×10^{-2}	782.5±19.8	0.998
500 × 15	1419	0.131	1399.6±30.3	0.952	1.2×10^{-3}	1429.3±15.4	0.999
700 × 15	1633	0.114	1619.0±18.3	0.991	5.3×10^{-4}	1646.8±21.5	0.999
1000 × 15	1826	0.197	1743.6±36.5	0.919	1.5×10^{-4}	1835.8±21.9	0.996

Table S17 Summary of the related parameters obtained via Langmuir and Freundlich isotherm models for iodine adsorption from iodine/cyclohexane solution by **ZIF-90** and **ZIF-90-I**–**ZIF-90-III**.

Compounds	Langmuir isotherm model			Freundlich isotherm model		
	K_L(L/mg)	Q_{max} (mg/g)	R^2	K_F (mg/g)	1/n	R^2
ZIF-90	235.1	569.2	0.982	45.9	0.32	0.971
ZIF-90-I	41.1	1036.4	0.960	131.7	0.27	0.868
ZIF-90-II	32.4	1444.2	0.951	238.6	0.26	0.912
ZIF-90-III	22.8	1795.4	0.959	666.3	0.15	0.889

Table S18 Calculated transferred charges (CT) from clusters to iodine molecules and corresponding binding energies (ΔE).

Compounds	CT (e)	ΔE (eV)
ZIF-90	−0.172	−0.664
ZIF-90-mono	−0.183	−0.687
ZIF-90-bis	−0.134	−0.574

References

1. Tang, Y.; Huang, H.; Li, J.; Xue, W.; Zhong, C. IL-induced formation of dynamic complex iodide anions in IL@MOF composites for efficient iodine capture. *J. Mater. Chem. A*, **2019**, *7*, 18324–18329.

2. Qi, B.; Liu, Y.; Zheng, T.; Gao, Q.; Yan, X.; Jiao, Y. and Yang, Y. Highly efficient capture of iodine by Cu/MIL-101. *J. Solid State Chem.*, **2018**, *258*, 49–55.

3. Guo, B.; Li, F.; Wang, C.; Zhang, L. and Sun, D. A rare (3,12)-connected zirconium metal–organic framework with efficient iodine adsorption capacity and pH sensing. *J. Mater. Chem. A*, **2019**, *7*, 13173–13179.

4. Marshall, R. J.; Griffin, S. L.; Wilson, C. and Forgan, R. S. Stereoselective halogenation of integral unsaturated C-C bonds in chemically and mechanically robust Zr and Hf MOFs. *Chem. Eur. J.*, **2016**, *22*, 4870–4877.

5. Said, A.; Gao, C.; Liu, C.; Niu, H.; Wang, D.; Liu, Y.; Du, L.; Tung, C. H.; Wang, Y. A mesoporous lead-doped titanium oxide compound with high performance and recyclability in I_2 uptake and photocatalysis. *Inorg. Chem.*, **2022**, *61*, 586–596.

6. Chen, P.; He, X.; Pang, M.; Dong, X.; Zhao, S.; Zhang, W. Iodine capture using Zr-based metal−organic frameworks (Zr-MOFs): adsorption performance and mechanism. *ACS Appl. Mater. Interfaces*, **2020**, *12*, 20429–20439.

7. Yao, R. X.; Cui, X.; Jia, X. X.; Zhang, F. Q. and Zhang, X. M. A luminescent Zinc(II) metal−organic framework (MOF) with conjugated π-electron ligand for high iodine capture and nitro-explosive detection. *Inorg. Chem.*, **2016**, *55*, 9270–9275.

8. Ohtsu, H.; Kim, J.; Kanamaru, T.; Inoue, D.; Hashizume, D.; Kawano, M. Stepwise observation of iodine diffusion in a flexible coordination network having dual interactive sites. *Inorg. Chem.*, **2021**, *60*, 13727–13735.

9. Sava, D. F.; Chapman, K. W.; Rodriguez, M. A.; Greathouse, J. A.; Crozier, P. S.; Zhao, H.; Chupas P. J. and Nenoff, T. M. Competitive I_2 sorption by Cu-BTC from humid gas streams. *Chem. Mater.*, **2013**, *25*, 2591–2596.

10. Brunet, G.; Safin, D. A.; Aghaji, M. Z.; Robeyns, K.; Korobkov, I.; Woo, T. K. and Murugesu, M. Stepwise crystallographic visualization of dynamic guest binding in a nanoporous framework. *Chem. Sci.*, **2017**, *8*, 3171–3177.

11. Zhang, X.; Silva, I. Da; Godfrey, H. G. W.; Callear, S. K.; Sapchenko, S. A.; Cheng, Y.; Vitórica-Yrezábal, I.; Frogley, M. D.; Cinque, G.; Tang, C. C.; Giacobbe, C.; Dejoie, C.; Rudić, S.; Ramirez-Cuesta, A. J.; Denecke, M. A.; Yang, S. and Schröder, M. Confinement of iodine molecules into triple-helical chains within robust metal−organic frameworks. *J. Am. Chem. Soc.*, **2017**, *139*, 16289–16296.

12. Wang, L.; Chen, P.; Dong, X.; Zhang, W.; Zhao, S.; Xiao, S.; Ouyang, Y. Porous MOF-808@PVDF beads for removal of iodine from gas streams. *RSC Adv.*, **2020**, *10*, 44679–44687.

13. Hughes, J. T.; Sava, D. F.; Nenoff, T. M. and Navrotsky, A.; Thermochemical evidence for strong iodine chemisorption by ZIF-8. *J. Am. Chem. Soc.* **2013**, *135*, 16256–16259.

14. Li, Z. J.; Guo, S.; Lu, H.; Xu, Y.; Yue, Z.; Weng, L.; Guo, X.; Lin, J.; Wang, J.-Q. Unexpected structural complexity of thorium coordination polymers and polyoxo cluster built from simple formate ligands. *Inorg. Chem. Front*., **2020**, *7*, 260–269.

15. Leloire, M.; Walshe, C.; Devaux, P.; Giovine, R.; Duval, S.; Bousquet, T.; Chibani, S.; Paul, J. F.; Moissette, A.; Vezin, H.; Nerisson, P.; Cantrel, L.; Volkringer, C.; Loiseau, T. Capture of gaseous iodine in isoreticular Zirconium-based UiO-n metal-organic frameworks: influence of amino functionalization, DFT calculations, Raman and EPR spectroscopic investigation. *Chem. Eur. J.*, **2022**, *28*, e202104437–e202104453.

16. Wang, X.; Zhang, H.; Qi, C.; Zhou, F.; Ni, L.; Chen, S.; Qi, J.; Wang, C.; Zheng, T.; Li, J. Hydrangea-like architectures composed of Zr-based metal–organic framework nanosheets with enhanced iodine capture. *Dalton Trans.*, **2021**, *50*, 16468–16472.

17. Wang, L.; Li, T.; Dong, X.; Pang, M.; Xiao, S.; Zhang, W. Thiophene-based MOFs for iodine capture: effect of pore structures and interaction mechanism. *Chem. Eng. J.*, **2021**, *425*, 130578–130586.

18. Wu, K.; Huang, Y. L.; Zheng, J.; Luo, D.; Xie, M.; Li, Y. Y.; Lu, W.; Li, D. A microporous shp-topology metal–organic framework with an unprecedented high-nuclearity Co_{10}-cluster for iodine capture and histidine detection. *Mater. Chem. Front.* **2021**, *5*, 4300–4309.

19. Luo, D.; Wang, F.; Liu, C.-H.; Wang, S.-T.; Sun, Y. Y.; Fang, W. H.; Zhang, J. Combination of aluminum molecular rings with chemical reduction centers for iodine capture and aggregation. *Inorg. Chem. Front.*, **2022**, *9*, 4506–4516.

20. Banerjee, D.; Chen, X.; Lobanov, S. S.; Plonka, A. M.; Chan, X.; Daly, J. A.; Kim, T.; Thallapally, P. K. and Parise, J. B. Iodine adsorption in metal organic frameworks in the presence of humidity. *ACS Appl. Mater. Interfaces*, **2018**, *10*, 10622–10626.

21. Valizadeh, B.; Nguyen, T. N.; Smit, B. and Stylianou, K. C. Porous metal–organic framework@polymer beads for iodine capture and recovery using a gas-sparged column. *Adv. Funct. Mater*., **2018**, *28*, 1801596–1801601.

22. Mao, P.; Qi, B.; Liu, Y.; Zhao, L.; Jiao, Y.; Zhang, Y.; Jiang, Z.; Li, Q.; Wang, J.; Chen, S. and Yang, Y. Ag^{II} doped MIL-101 and its adsorption of iodine with high speed in solution. *J. Solid State Chem*., **2016**, *237*, 274–283.

23. Hashemi, L. andMorsali, A. A new lead(II) nanoporous three-dimensional coordination polymer: pore size effect on iodine adsorption affinity. *CrystEngComm*, **2014**, *16*, 4955–4958.

24. Safarifard, V. and Morsali, A. Influence of an amine group on the highly efficient reversible adsorption of iodine in two novel isoreticular interpenetrated pillared-layer microporous metal–organic frameworks. *CrystEngComm*, **2014**, *16*, 8660–8663.

25. Feng, Y.; Yang, P.; Li, Y. and Gu, J. J. AgNPs-containing metal−organic frameworks for the effective adsorption and immobilization of radioactive iodine. *Chem. Eng. Data,* **2020**, *65*, 1986–1992.

26. Liu, M. D.; Abrahams, B. F.; Ren, Z. G.; Lang, J. P. A 3D $[WS_4Cu_4]^{2+}$ cluster-based material with high iodine uptake capability. *Dalton Trans.* **2019**, *48*, 6695–6699.

27. Zheng, H. W.; Yang, D.-D.; Liang, Q.-F.; Liu, Y.-P.; Shan, J.-H.; Liu, Q.-Q.; Tan, H.-W.; Chen, L.; Zheng, X.-J. A diamond-like cuprous coordination polymer based on the $[Cu_8I_6]^{2+}$ cluster with multistimuli-responsive luminescence and iodine adsorption behavior. *J. Mater. Chem. C.*, **2022**, *10*, 3901–3907.

28. He, W. W.; Li, S. L.; Yang, G. S.; Lan, Y. Q.; Su, Z. M. and Fu, Q. Controllable synthesis of a non-interpenetrating microporous metal–organic framework based on octahedral cage-like building units for highly efficient reversible adsorption of iodine. *Chem. Commun.*, **2012**, *48*, 10001–10003.

29. Shi, B. B.; Pei, R. Z.; Chen, A. W.; Wang, C.; Ma, Y. M. and Yin, Z. A rigid and porous metal-organic frameworks with 1D rhombus channels and double walls: Selective adsorption of CO_2 over N_2, iodine capture, and fluorescence. *Inorg. Chem. Commun.*, **2019**, *102*, 147–151.

30. Choi, H. J. and Suh, M. P. Dynamic and redox active pillared bilayer open framework: single-crystal-to-single-crystal transformations upon guest removal, guest exchange, and framework oxidation. *J. Am. Chem. Soc.*, **2004**, *126*, 15844–15851.

31. He, T.; Xu, X.; Ni, B.; Lin, H.; Li, C.; Hu, W. and Wang, X. Metal–organic framework based microcapsules. *Angew. Chem. Int. Ed.,* **2018**, *57*, 10148–10152.

32. Li, H.; Li, Y.; Li, B.; Liu, D. and Zhou, Y. Highly selective anchoring silver nanoclusters on MOF/SOF heterostructured framework for efficient adsorption of radioactive iodine from aqueous solution. *Chemosphere,* **2020**, *252*, 126448–126459.

33. Yu, F.; Li, D. D.; Cheng, L.; Yin, Z.; Zeng, M. H. and Kurmoo, M. Porous supramolecular networks constructed of one-dimensional metal−organic chains: carbon dioxide and iodine capture. *Inorg. Chem.*, **2015**, *54*, 1655–1660.

34. Zhang, H. M.; Wu, H.; Liu, Y. Y.; Yang, J.; Kang, D. W. and Ma, J. F. Syntheses, structures, gas adsorption and reversible iodine adsorption of two porous Cu(II) MOFs. *CrystEngComm,* **2015**, *17*, 1583–1590.

35. Deshmukh, M. S.; Chaudhary, A.; Zolotarev, P. N.; Boomishankar, R. A 3D coordination network built from $Cu^{II}_4Cl_3(H_2O)_2$ linear clusters and tetrapyridyl tetrahedral silane ligands: reversible iodine uptake and friedel−crafts alkylation reactions. *Inorg. Chem*., **2017**, *56*, 11762–11767.

36. Li, Z. J.; Yue, Z.; Ju, Y.; Wu, X.; Ren, Y.; Wang, S.; Li, Y.; Zhang, Z. H.; Guo, X.; Lin, J.; Wang, J. Q. Ultrastable thorium metal−organic frameworks for efficient iodine adsorption. *Inorg. Chem.*, **2020**, *59*, 4435–4442.

37. Liu, C. H.; Fang, W. H.; Sun, Y.; Yao, S.; Wang, S. T.; Lu, D.; Zhang, J. Designable assembly of aluminum molecular rings for sequential confinement of iodine molecules. *Angew. Chem. Int. Ed*., **2021**, *60*, 21426–21433.

38. Cui, P.; Ren, L.; Chen, Z.; Hu, H.; Zhao, B.; Shi, W. and Cheng, P. Temperature-controlled chiral and achiral copper tetrazolate metal−organic frameworks: syntheses, structures, and I_2 adsorption. *Inorg. Chem.*, **2012**, *51*, 2303–2310.

39. Zhang, Z. J.; Shi, W.; Niu, Z.; Li, H. H.; Zhao, B.; Cheng, P.; Liao, D. Z. and Yan, S. P. A new type of polyhedron-based metal–organic frameworks with interpenetrating cationic and anionic nets demonstrating ion exchange, adsorption and luminescent properties. *Chem. Commun.*, **2011**, *47*, 6425–6427.

40. Yin, Z.; Wang, Q. X.; Zeng, M. H. Iodine release and recovery, influence of polyiodide anions on electrical conductivity and nonlinear optical activity in an interdigitated and interpenetrated bipillared-bilayer metal−organic framework. *J. Am. Chem. Soc.*, **2012**, *134*, 4857–4863.

41. Wang, G. Q.; Huang, J. F.; Huang, X. F.; Deng, S. Q.; Zheng, S. R.; Cai, S. L.; Fan, J.; Zhang, W.-G. A hydrolytically stable cage-based metal–organic framework containing two types of building blocks for the adsorption of iodine and dyes. *Inorg. Chem. Front.*, **2021**, *8*, 1083–1092.

42. Falaise, C.; Volkringer, C.; Facqueur, J.; Bousquet, T.; Gasnot, L. and Loiseau, T. Capture of iodine in highly stable metal–organic frameworks: a systematic study. *Chem.Commun*., **2013**, *49*, 10320–10322.

43. Parshamoni, S.; Sanda, S.; Jena, H. S.; Konar, S. Tuning CO_2 uptake and reversible iodine adsorption in two isoreticular mofs through ligand functionalization. *Chem. Asian J.*, **2015**, *10*, 653–660.

44. Sun, F.; Yin, Z.; Wang, Q. Q.; Sun, D.; Zeng, M. H. and Kurmoo, M. Tandem postsynthetic modification of a metal–organic framework by thermal elimination and subsequent bromination: effects on absorption properties and photoluminescence. *Angew. Chem. Int. Ed.,* **2013**, *52*, 4538–4543.

45. Yao, S.; Sun, X.; Liu, B.; Krishna, R.; Li, G.; Huo, Q. and Liu, Y. Two heterovalent copper–organic frameworks with multiple secondary building units: high performance for gas adsorption and separation and I_2 sorption and release. *J. Mater. Chem. A,* **2016**, *4*, 15081–15087.

46. Gao, Q.; Liu, Y.; Jiao, Y.; Yang, Y.; Zhang, X.; Wang, P.; Chen, J.; Gao, Q.; Zhang, X.; Liu, Y.; Wang, P.; Jiao, Y. and Yang, Y. Nanometer mixed-valence silver oxide enhancing adsorption of ZIF-8 for removal of iodide in solution. *Sci. Total Environ.*, **2018**, *646*, 634–644.

47. Rachuri, Y.; Bisht, K. K.; Parmar, B.; Suresh, E. Luminescent MOFs comprising mixed tritopic linkers and Cd(II)/Zn(II) nodes for selective detection of organic nitro compounds and iodine capture. *J. Solid State Chem.*, **2015**, *223*, 23–31.

48. Lang, J. P.; Xu, Q. F.; Yuan, R. X. and Abrahams, B. F. {[WS_4Cu_4(4,4'-bpy)$_4$][$WS_4Cu_4I_4$(4,4'-bpy)$_2$]}$_\infty$—An unusual 3d porous coordination polymer formed from the preformed cluster [Et_4N]$_4$[$WS_4Cu_4I_6$]. *Angew.Chem. Int. Ed.,* **2004**, *43*, 4741–4745.

49. Liu, Q. K.; Ma, J. P. and Dong, Y. B. Highly efficient iodine species enriching and guest-driven tunable luminescent properties based on a cadmium(II)-triazole MOF. *Chem. Commun*., **2011**, *47*, 7185–7187.

50. Liu, J.; Xiao, R.; Wong, Y. L.; Zhou, X. P.; Zeller, M.; Hunter, A. D.; Fang, Q.; Liao, L. and Xu, Z. Made in water: a stable microporous Cu(I)-carboxylate framework (CityU-7) for CO_2, water, and iodine uptake. *Inorg. Chem.*, **2018**, *57*, 4807–4811.

51. Wang, J.; Luo, J.; Luo, X.; Zhao, J.; Li, D. S.; Li, G.; Huo, Q. and Liu, Y. Assembly of a three-dimensional metal−organic framework with copper(i) iodide and 4-(pyrimidin-5-yl) benzoic acid: controlled uptake and release of iodine. *Cryst. Growth Des*., **2015**, *15*, 915–920.

52. Mani, P.; Mandal, N.; Roopesh, M.; Gopalakrishnan, H.; Datta, A. and Mandal, S. Enhancement in electrical conductivity of a porous indium based metal–organic framework upon I_2 uptake: combined experimental and theoretical investigations. *J. Mater. Chem. C*, **2020**, *8*, 4836–4842.

53. Feng, S. S.; Bai, Y. T.; Zhu, J. L.; Lu, L. P. and Zhu, M. L. Irreversible solvent-assisted structural transformation in 3D metal-organic frameworks: Structural modification and enhanced iodine-adsorption properties. *Spectrochim. Acta, Part A,* **2018**, *205*, 139–145.